

AN AQUIFER-WELL COUPLED MODEL

A refined implementation of wellbore boundary conditions in three-dimensional, heterogeneous formations

by

Matthew D. Cyr

A thesis submitted to the Department of Civil Engineering
in conformity with the requirements for
the degree of Master of Science

Queen's University

Kingston, Ontario, Canada

December, 2007

Copyright © Matthew D. Cyr, 2007

Abstract

This paper presents modifications to two widely used numerical groundwater flow models in an effort to improve upon the interaction between a well of finite length and conductivity with the surrounding formation. The first objective is to discard the common assumptions about flux- or head-based boundary conditions along the well screen by coupling pipe flow hydraulics and groundwater flow. The second objective is to avoid restricting the wellbore hydraulics to a single flow regime. Five flow regimes (laminar through rough-turbulent), based on Reynolds number and pipe roughness, are considered. The modifications are integrated into the highly versatile, well-documented and well-tested models *HydroGeoSphere* (finite-element/finite-difference) and USGS MODFLOW (finite-difference). Verification of the algorithm and code is performed by comparing results to: 1) the idealized, analytical Theis solution; 2) the original, unmodified code; and 3) the results of a third party numerical solution that also accounts for variable frictional wellbore losses. Results highlight the inadequacy of either a uniform flux or a uniform head assumption along the wellbore. The solution also tends to produce much steeper hydraulic gradients in those portions of the aquifer nearest the pump intake than have previously been predicted. Systems most affected by in-well hydraulic losses include those for which well screen is long, pumping rate is large, pipe diameter is small, pipe roughness is large (either through design or aging) and aquifer conductivity is high. Improved modeling of the non-linear hydraulic conditions within the well screen can particularly influence the interpretation of wellbore flowmeter and tracer tests, leading to more precise knowledge of the variation of local aquifer hydraulic conductivity along well screens. Aquifer drawdown curves, solute transport and inflow

velocities will also be influenced, which can impact capture zones and remediation costs. Given that the solution is incorporated within the HydroGeoSphere and MODFLOW models, it presents the additional advantage over existing approaches of offering a wide range of modeling capabilities, such as three-dimensional flow, arbitrary well inclination and surface-subsurface flow integration.

Acknowledgements

I would like to thank S. David Graber for his advice and his interest in my work. He also graciously provided helpful review and comments.

Tony Falkland generously provided support and some valuable experience along the way.

Rob McLaren kindly supplied frequent insights into the workings of the HydroGeoSphere code.

Thanks to my advisor, Kent Novakowski, for his help and patience.

Thanks to my dad for his support and corrections.

Thanks also to my wife, Carolyn, for her support and patience.

Table of Contents

Abstract.....	ii
Acknowledgements	iv
Table of Contents	v
List of Tables	vii
List of Figures.....	viii
Chapter 1 Introduction.....	1
1.1 References	6
Chapter 2 An aquifer-well coupled model: a refined implementation of wellbore boundary conditions in three-dimensional, heterogeneous formations.	8
2.1 Introduction.....	9
2.2 Theoretical development	16
2.2.1 Problem statement.....	16
2.2.2 Pipe flow	18
2.2.3 Numerical formulation.....	22
2.2.3.1 Pipe flow regimes	22
2.2.3.2 Numerical models	26
2.3 Code Verification	28
2.3.1 HydroGeoSphere.....	28
2.3.2 MODFLOW	32
2.3.3 Comparison to the numerical model of Chen et al. (2003).....	33
2.4 Results and discussion	36
2.4.1 Grid design.....	36
2.4.2 Sensitivity analysis.....	38
2.4.3 Contour predictions.....	42
2.4.4 Comparison to the semi-analytical model of Tarshish (1992).....	45
2.5 Model limitations and future research.....	48

2.5.1	Limitations and suggested modifications.....	48
2.5.2	Momentum exchange and orifice discharge	52
2.6	Summary and conclusions.....	53
2.7	References	56
Chapter 3	Summary and conclusions.....	60
Appendix I:	<i>HydroGeoSphere</i> modifications	63
Appendix II:	MODFLOW-2000 modifications	66
Appendix III:	HydroGeoSphere grid verification	69
Appendix IV:	Note on wellbore storage in <i>HydroGeoSphere</i>	74

List of Tables

Table 1 Aquifer properties used for model comparison between the Theis solution and the unmodified <i>HGS</i> code.....	29
Table 2 Percent difference in drawdown between the modified and original versions of <i>HGS</i> for selected observation points. The maximum difference for each point is highlighted. r is the radial distance from the well node, which represents the center of the well, to the point of observed drawdown.....	31
Table 3 Sensitivity of solution to aquifer hydraulic conductivity ($K_1 = 2.3 \times 10^{-5}$, $K_2 = 2.3 \times 10^{-4}$ and $K_3 = 2.3 \times 10^{-3}$ m/s): (a) percentage of flow entering the half of the well nearest the pump intake; and (b) hydraulic head loss (in meters) along the full length of the well screen. Pumping rate, Q , is 4×10^{-3} m ³ /s (240 L/min), well screen diameter, D , is 0.1m and absolute roughness, e , is a negligible 1×10^{-7} m at $t = 1.34 \times 10^6$ s. The solution using the original <i>HGS</i> code is also presented for comparison.....	41
Table 4 List of selected <i>HGS</i> grids tested with the Theis solution.....	74

List of Figures

Figure 1 Example boundary conditions assigned to a wellbore in a porous medium pumped from one end at a rate Q , showing various hydraulic head (h) and flux (q) distributions along its length.....	2
Figure 2 Horizontal well installed to maximize plume contact (USDOE, 1998).	3
Figure 3 Flow chart for flow regime selection. f represents the bisectional root finding function of equation (2) to locate Re and g represents the nested bisectional root finding function to find f_D	26
Figure 4 Flow chart for entire computational process in the modified versions of: a) <i>HydroGeoSphere</i> and b) MODFLOW.....	27
Figure 5 Drawdown at radial distances of 1, 2 and 8 m for pumping in a Theis aquifer. With a moderate pumping rate of $4 \times 10^{-3} \text{ m}^3/\text{s}$ (240 L/min) and a large well screen diameter ($D=0.4 \text{ m}$), frictional losses are minimized along the pipe and so flow within the wellbore remains close to laminar and the modified <i>HydroGeoSphere</i> solution matches closely the Theis solution. Data from the <i>HGS</i> solution is taken at the aquifer top.	30
Figure 6 Comparison of the modified <i>HGS</i> solution and that of Chen et al. (2003) for drawdown distribution along a horizontal well screen. The data selected is from a published graph (fig. 2) and is accurate to within 0.1 m. The original, unmodified <i>HGS</i> solution is included for reference.	34
Figure 7 Comparison of the modified <i>HGS</i> solution and that of Chen et al. (2003) for well flux per unit length along a horizontal well screen. The data selected is from a published graph (fig. 3) and is accurate to within $1.7 \times 10^{-6} \text{ m}^2/\text{s}$. The original, unmodified <i>HGS</i> solution is included for reference.	35
Figure 8 Comparison of the modified <i>HGS</i> solution and that of Chen et al. (2003) for well conductivity (K_w) distribution along a horizontal well screen. The data selected is from a published graph (fig. 4) and is accurate to within 12 m/s. The original, unmodified <i>HGS</i> solution is included for reference.	35
Figure 9 Drawdown along the well screen, indicating sensitivity of the modified <i>HGS</i> solution (mod) to screen diameter ($D_1 = 0.2 \text{ m}$, $D_2 = 0.1 \text{ m}$, $D_3 = 0.05 \text{ m}$) for a pumping rate of $4 \times 10^{-3} \text{ m}^3/\text{s}$ (240 L/min) and a negligible roughness, $e = 1 \times 10^{-7} \text{ m}$. The pump intake is located at node location 300 m. The results using the original code solution (org) are also presented for comparison.	39
Figure 10 Flux per unit length of well screen, as a percentage of total pumping rate, Q , indicating sensitivity of the modified <i>HGS</i> solution (mod) to pumping rate, Q , for a screen diameter of 0.1m and a negligible absolute roughness, $e = 1 \times 10^{-7} \text{ m}$, for pumping rates $Q1 = 1 \times 10^{-3} \text{ m}^3/\text{s}$ (60 L/min) and $Q2 = 4 \times 10^{-2} \text{ m}^3/\text{s}$ (2400 L/min).	

The results using the original code solution (org) are also presented for comparison.
 39

Figure 11 Plan view of domain used to investigate aquifer head contours. All figures in meters. Domain dimensions selected from model used in Mohamed and Rushton (2006), though grid discretization and some boundary conditions are different. 42

Figure 12 Highly asymmetrical hydraulic head contours generated using the modified version of *HGS* which includes well screen losses based on multiple flow regimes. The well screen is indicated by the horizontal line centered on location 0, 0. All figures in meters. Absolute roughness is equal to 8×10^{-4} m. 43

Figure 13 Hydraulic head contours generated using the original version of *HGS* which includes well screen losses based on laminar flow only. The well screen is indicated by the horizontal line centered on location 0, 0. All figures in meters. 44

Figure 14 Reynolds number (Re) and hydraulic conductivity (K_w) at each well node along the wellbore generated with the modified *HGS* code for the contour prediction simulation. Flow regime labels point to the well segments in which the particular flow first appears while moving toward the pumping node, at node location +150 m. 45

Figure 15 Hydraulic head along the well screen for the steady state simulation presented in Tarshish (1992), where water is pumped from $x = 0$. Results are presented from the original publication, along with the modified *HGS* solution (Modified *HGS* - 1) for a well diameter (D) of 0.15 m and a negligible value of absolute roughness ($e = 1 \times 10^{-8}$ m). *HGS* results produce flow that is smooth, while Tarshish assumes static turbulent flow. Modified *HGS* - 2 represents results where the code has been altered to treat flow as strictly turbulent. Original, unmodified *HGS* results (Original *HGS*) are also presented for comparison..... 46

Figure 16 Flux per unit length of well screen. See Figure 15 for details..... 47

Figure 17 Drawdown at radial distances of 0.98225 m and 40.87747 m for pumping in a Theis aquifer. g10 corresponds to the *HGS* solution using a horizontal grid configuration of 53x53 nodes. 71

Figure 18 Flux per unit length of wellbore at $t = 42949672$ s, for vertical grid discretization of 11, 21, 31 and 61 nodes; g8 was used for horizontal discretization. No significant variation in flux is observed between grids for this and other times. 72

Figure 19 Hydraulic head along the wellbore at $t = 42949672$ s, for vertical grid discretization of 11, 21, 31 and 61 nodes; g8 was used for horizontal discretization. No significant variation in head is observed between grids for this and other times. 72

Figure 20 Drawdown at a radial distance of 52 m for pumping in a Theis aquifer using three different vertical node configurations. 73

Figure 21 Flux per well node for various horizontal grid discretization at $t = 42949672$ s. The same pattern emerged at several simulation times. 73

Figure 22 Drawdown within the well screen for various horizontal grid discretization at $t = 42949672$ s. The same pattern emerged at several simulation times..... 74

Figure 23 Drawdown at radial distances of 1, 2 and 8 m for pumping in a Theis aquifer, following the code verification example in section 2.3.1. A caisson radius of zero is used in order to remove wellbore storage from the *HGS* calculations. The Theis solution is plotted against HGS solutions both with (*HGS + storage*) and without (*HGS*) wellbore storage..... 75

Chapter 1 Introduction

The two traditional boundary conditions used with pumping well solutions include the application of a uniform head (Figure 1a) or a uniform flux (Figure 1b) distribution along the well screen (Park and Zhan, 2002). Studies such as Cooley and Cunningham (1979) and Korom et al. (2003) show, theoretically and experimentally, that water does not enter the wellbore uniformly but concentrates near the pumped end. Hantush (1964) suggests that actual wellbore flow conditions create a realistic situation that lies somewhere between these two extremes and that a mixed-type boundary condition on the well screen is more appropriate. Cheng et al. (2005) have shown that such a mixed-type boundary condition leads to results that are in fact significantly different and more extreme than those resulting from simulations making either of the aforementioned assumptions.

Inflow and hydraulic head along the well screen axis will not be uniform due to energy loss within and around the well screen as water flows toward the pump intake (Figure 1c). Well screens can have large, commonly ignored hydraulic resistances that can significantly influence well characteristics and thus inclusion of these may be warranted for well design and evaluation (Tarshish, 1992).

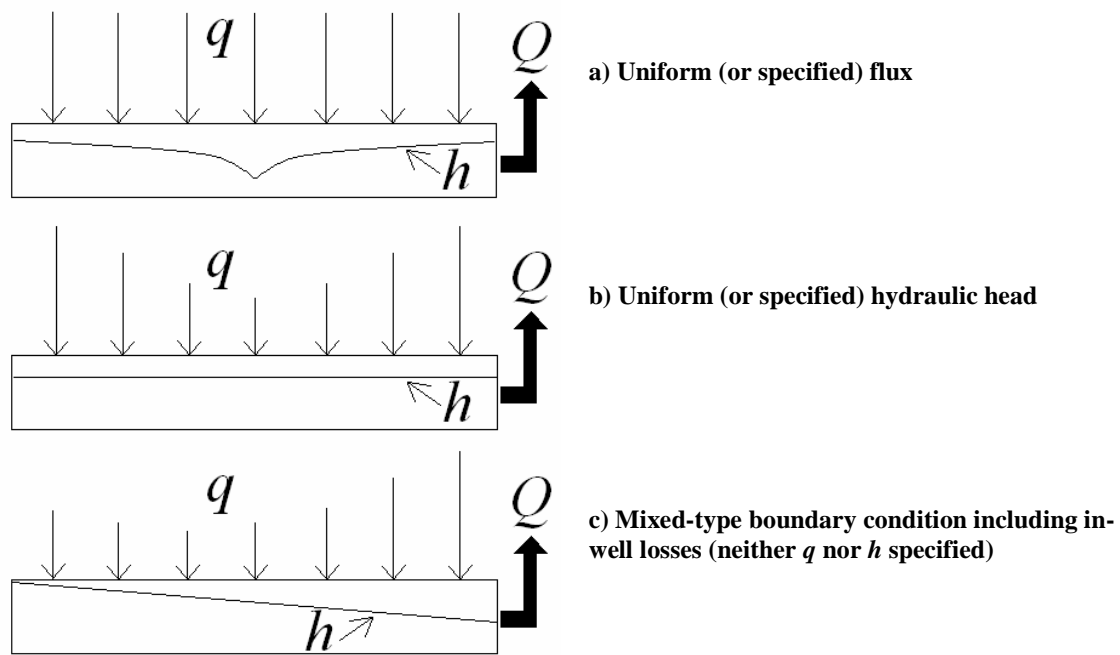


Figure 1 Example boundary conditions assigned to a wellbore in a porous medium pumped from one end at a rate Q , showing various hydraulic head (h) and flux (q) distributions along its length.

Among other factors, long well screens, large wellbore flow rates, high aquifer conductivities and small-diameter well screens can lead to significant frictional losses within a well (Szekely, 1992). Although a mixed-type boundary solution may be warranted for wells of any inclination, horizontal wells, which are being increasingly considered for groundwater remediation (Zhan, 1999), will be especially influenced, having longer screens. Modern directional drilling has allowed horizontal wells to be drilled up to several kilometers in length (Steward and Jin, 2001).

In many well applications, keeping the wellbore in contact with a targeted subsurface zone is critical, and often best achieved with a horizontal well. Many natural formations can be more extensive laterally than vertically, allowing horizontal wells to offer the advantage over vertical ones of having a longer contact length with their targeted aquifer

and therefore intercepting a larger planar area (Sawyer and Lieuallen-Dulum, 1998). As a result, they may be more efficient and cost effective than vertical wells in certain remediation scenarios (O'Neil et al, 1999). Contaminant plumes tend to be distributed as flat, vertically thin, broad layers which can be skimmed from the tops of thick aquifers (Schafer 1996). Horizontal wells can be placed parallel to such plumes, vastly increasing the per-well zone of influence and capture (Figure 2), leading to increased recovery efficiency and shorter remediation times (USACE, 1996; Allouche et al., 1998). Additionally, horizontal wells are also used to distribute aquifer drawdown more uniformly over a long distance to prevent upconing in small-island, coastal and inland aquifers underlain by seawater (Falkland, 1991; Das Gupta, 1983; Hunt, 1985; Saeed et al., 2002).

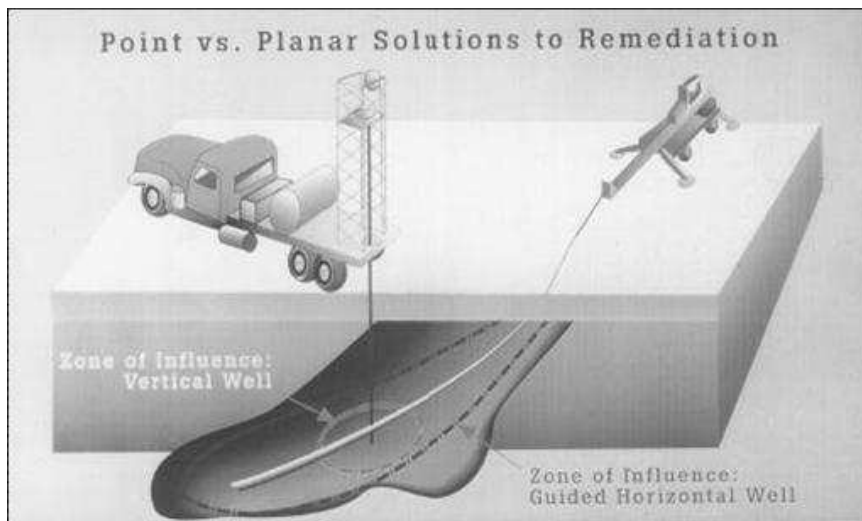


Figure 2 Horizontal well installed to maximize plume contact (USDOE, 1998).

Field and numerical results from Mohamed and Rushton (2006) indicate that a horizontal well should neither be represented by a constant head nor a uniform flux boundary

condition. They found hydraulic heads in the pumping caisson to be significantly lower than at the well ends. In addition, fluxes along the well screen were found to be sensitive to pumping rate variations, sometimes with the maximum inflow 1.5 times the minimum. Chen et al. (2003) obtain similar results from their numerical and physical models of a horizontal well.

The purpose of this research is to simulate flow in a porous medium penetrated by a finite length well, using the equations of flow in the aquifer coupled to flow along the axis of the well screen. To simulate wellbore flow, an equivalent hydraulic conductivity is assigned to each well cell/node based on in-well flow conditions related to pipe flow regimes and pipe friction. As there can be five possible flow regimes (laminar, critical, smooth, transitional or rough turbulent), an iterative process is performed to determine the appropriate equation governing pipe flow, as defined by the flow Reynolds number inside the well. The goal is not to create an entirely new, stand-alone model (such as that of Chen et al. (2003) or Cheng et al. (2005)), but to make use of existing numerical solvers, creating a more complete, versatile package. This was accomplished through the enhancement of two widely applied numerical models, MODFLOW, the U.S. Geological Survey's three-dimensional, finite-difference flow model, and *HydroGeoSphere*, a three-dimensional, finite-element/finite-difference, fully integrated surface-subsurface flow and transport model. This study also provides a suggested method for including the remaining two hydraulic loss mechanisms, related to screen orifices and momentum exchange within the well.

Refining the flow treatment at the well screen should be especially beneficial for tracer and flowmeter tests, or wherever in-well hydraulics is important (Cassiani and Kabala, 1998; Halford, 2000). This usefulness is highlighted for such circumstances as quantifying aquifer heterogeneity, where Sudicky et al. (1995) show that groundwater flux distribution along a well screen is highly correlated to the local hydraulic conductivity of the well's surrounding porous medium. Similarly, this usefulness may translate into enhanced understanding of near-well solute transport and capture details for remediation scenarios. Increased accuracy of hydraulic head and flux distribution along the well screen also allows for more informed decisions to be made about optimizing screen (diameter, length and material) and pumping rate selection where inflow velocities, sustainability and well efficiencies are of concern (Korom et al., 2003). In many circumstances, well screen entrance velocities must be kept below a certain critical value in order to prevent sand intake and compaction of fine particles around the well, which can lead to increased skin conductivity and reduced well efficiency (VonHofe and Helweg, 1998).

1.1 References

- Allouche, E. N., S. T. Ariaratnam and K. W. Biggar, 1998. Environmental remediation using horizontal directional drilling: Applications and modeling. *Prac. Period. Hazard. Toxic Radioact. Waste Manage., ASCE*, **2**(3), 93-99.
- Cassiani, G., and Z. J. Kabala, 1998. Hydraulics of a partially penetrating well: solution to a mixed-type boundary value problem via dual integral equations. *J. of Hydrology*, **211**, 100-111.
- Chen C., J. Wan, and H. Zhan, 2003. Theoretical and experimental studies of coupled seepage-pipe flow to a horizontal well. *J. of Hydrology*, **281**, 159-171.
- Cheng, Y., D. A. McVay and W. J. Lee, 2005. BEM for 3D unsteady-state flow problems in porous media with a finite-conductivity horizontal wellbore. *Applied Numerical Mathematics*, **53**, 19-37.
- Cooley, R. L. and A. B. Cunningham, 1979. Consideration of total energy loss in theory of flow to wells. *J. of Hydrology*, **43**, 161-184.
- Das Gupta, A., 1983. Steady interface upconing beneath a coastal infiltration gallery. *Ground Water*, **21**(4), 465-474.
- Falkland, A.C., editor, 1991. Hydrology and water resources of small islands, a practical guide. Studies and reports on hydrology No 49. Prepared by A. Falkland and E. Custodio with contributions from A. Diaz Arenas and L. Simler and case studies submitted by others. Paris, France, 435pp.
- Halford, K. J., 2000. Simulation and interpretation of borehole flowmeter results under laminar and turbulent flow conditions. International Symposium on Borehole Geophysics for Minerals, Geotechnical, and Groundwater Applications, vol.7, pp.157-168.
- Hantush, M. S., 1964. Hydraulics of wells. In: *Advances in hydroscience*. Academic Press, New York, NY.
- Hunt, B., 1985. Seepage to collection gallery near seacoast. *Water Resources Research*, **21**(3), 311-316.
- Korom, S. F., K. F. Bekker and O. J. Helweg, 2003. Influence of pump intake location on well efficiency. *J. Hydrologic Engrg., ASCE*, **8**(4), 197-203.
- Mohamed, A. and K. Rushton, 2006. Horizontal wells in shallow aquifers: Field experiment and numerical model. *J. of Hydrology*, **329**, 98-109.

O'Neil, R. P., A. H. Smyth, J. May, and K. Preston, 1999. Horizontal vs. vertical wells; A comparison. *Water Well J.*, **53**, 34-40.

Park E. and H. Zhan, 2002. Hydraulics of a finite-diameter horizontal well with wellbore storage and skin effect. *Advances in Water Resources*, **25**, 389-400.

Saeed, M. M., M. Bruen, and M. N. Asghar, 2002. A review of modeling approaches to simulate saline-upconing under skimming wells. *Nordic Hydrology*, **33**(2-3), 165-188.

Sawyer, C. S, and K. K. Lieuallen-Dulam, 1998. Productivity comparison of horizontal and vertical ground water remediation well scenarios. *Ground Water*, **36**(1), 98-103.

Schafer, D. C., 1996. Determining 3D capture zones in homogeneous, anisotropic aquifers. *Ground Water*, **34**(4), 628-639.

Steward, D. R., W. Jin, 2001. Gaining and losing sections of horizontal wells. *Water Resources Research*, **37**(11), 2677-2685.

Sudicky, E. A., A. J. A. Unger and S. Lacombe, 1995. A noniterative technique for the direct implementation of well bore boundary conditions in three-dimensional heterogeneous formations. *Water Resour. Res.*, **31**(2), 411-415.

Szekely, F., 1992. Pumping test data analysis in wells with multiple or long screens. *J. of Hydrology*, **132**, 137-156.

Tarshish, M., 1992. Combined mathematical model of flow in an aquifer-horizontal well system. *Ground Water*, **30**(6), 931-935.

USACE, 1996. Horizontal directional drilling for environmental applications. ETL 1110-1-178. US Army Corps of Engineers. December 10, 1110-1178.

USDOE, 1998. Horizontal wells – subsurface contaminants focus area. DOE/EM-0378. U.S. Department of Energy, Savannah River Site, Aiken, South Carolina.

VonHofe, F., and O. J. Helweg, 1998. Modeling Well Hydrodynamics. *J. Hydraulic Engrg., ASCE*, **124**(12), 1198-1202.

Zhan, H., 1999. Analytical study of capture time to a horizontal well. *Journal of Hydrology*, **217**, 46-54.

**Chapter 2 An aquifer-well coupled model: a refined
implementation of wellbore boundary conditions in three-
dimensional, heterogeneous formations.**

By: Matthew D. Cyr[†] and Kent S. Novakowski[†]

To be submitted to: *Journal of Hydrology*

[†]Department of Civil Engineering,
Queen's University, Kingston, Ontario, Canada, K7L 3N6

2.1 Introduction

The two traditional boundary conditions used with pumping well solutions include the application of a uniform head or a uniform flux distribution along the well screen (Park and Zhan, 2002). Studies such as Cooley and Cunningham (1979) and Korom et al. (2003) show, theoretically and experimentally, that water does not enter the wellbore uniformly but concentrates near the pumped end. Hantush (1964) suggests that actual wellbore flow conditions create a realistic situation that lies somewhere between these two extremes and that a mixed-type boundary condition on the well screen is more appropriate. Cheng et al. (2005) have shown that such a mixed-type boundary condition leads to results that are in fact significantly different and more extreme than those resulting from simulations making either of the aforementioned assumptions.

Inflow and hydraulic head along the well screen axis will not be uniform due to energy loss within and around the well screen as water flows toward the pump intake. Partial penetration will also influence the concentration of flow. Well screens can have large hydraulic resistances that can significantly influence well characteristics and thus inclusion of these may be warranted for well design and evaluation (Tarshish, 1992).

Field and numerical results from Mohamed and Rushton (2006) also indicate that a horizontal well should neither be represented by a constant head nor a uniform flux boundary condition. They found hydraulic heads in the pumping caisson to be significantly lower than at the well ends. In addition, fluxes along the well screen were found to be sensitive to pumping rate variations, sometimes with the maximum inflow

1.5 times the minimum. Chen et al. (2003) obtain similar results from their numerical and physical models of a horizontal well.

Among other factors, long well screens, large wellbore flow rates, high aquifer conductivities and small-diameter well screens can lead to significant frictional losses within a well (Szekely, 1992). Although a mixed-type boundary solution may be warranted for wells of any inclination, horizontal wells, which are being increasingly considered for groundwater remediation (Zhan, 1999), will be especially influenced, having longer screen lengths.

There are recent studies that solve the boundary value problem for horizontal and slanted wells such as the semi-analytical approach of Zhan and Zlotnik (2002) that uses a line sink with an assumed uniform flux distribution to represent the well. Despite providing the option to specify an arbitrary flux distribution along the well screen in this approach, the variable nature of pipe flow and the well-aquifer interaction cannot be accommodated. The same study points to small discrepancies between solutions with competing assumptions of either uniform head or uniform flux. For one simulation Zhan and Zlotnik (2002) specifically report less than 10% drawdown error at distances of less than five well diameters from the well end and less than 1% error beyond that. This analysis does not consider, however, hydraulic pipe losses that can impact aquifer head more significantly than the difference observed between these two ideal scenarios.

Mohamed and Rushton (2006) present a pseudo-3D, finite-difference numerical model for flow to a horizontal well, in a shallow, homogeneous aquifer. In this model, flow is assumed to be always turbulent, attributed to the impact of inflowing water through the well slots, and as such, frictional losses are accounted for through the use of only a single equation, that being the Hazen-Williams expression. Szekely (1992) suggests that hydraulic roughness of the screened portion of a well will be higher than the unscreened portion, but a review of a number of studies discussed in Graber (2004) suggest that inflow will have little influence on pipe friction (and hence flow conditions) in subsurface drains that generally have perforations that are small compared to axial flow cross section. It is likely, therefore, that a strictly rough turbulent flow assumption is not accurate. A unique feature of the Mohamed and Rushton model is the inclusion of an additional head loss component for flow through well screen orifices, by coupling a third equation to the equations of aquifer flow and pipe flow. Due to its single layer and two-dimensional nature, this model is computationally efficient, particularly for unconfined conditions, but is limited to uniform, thin aquifers.

Chen and Jiao (1999) present a quasi-three-dimensional solution for flow to a vertical well with a treatment for in-well hydraulics that identifies five flow regimes. The Darcy friction factor used in calculating an equivalent well hydraulic conductivity, however, must be read from Nikuradse's experimental curves when the flow regime falls outside of the laminar. This model is thus limited by the number of curves drawn for each type of pipe (based on relative roughness, e/D) from which to select friction values. Additionally, this adds an extra and impractical manual component to the calculations.

The authors report a satisfactory agreement between numerical model and field experiment. That is, for 420 simulated values of drawdown which varied between zero and one metres during a pumping test, 51% were within 0.05 m of experimental readings, while less than 1% were greater than 0.15 m of experimental readings. This is the only study in which this treatment is extended to observation wells.

Chen et al. (2003) present a similar treatment for horizontal wells, but use the explicit Blasius equation for flow in the smooth turbulent regime, and leave unspecified how the gaps are bridged from the laminar to the smooth turbulent regime and from the smooth turbulent to the rough turbulent regime. By using an explicit equation for flow in the smooth turbulent regime, an artificial jump is introduced between the smooth and rough flow regimes that is not observed experimentally. Any explicit equation is in fact only an approximation and additionally requires boundaries between flow regimes to be fixed that are otherwise flow-dependent. Despite reporting good agreement between physical and finite-difference numerical models, this study presents limitations where greater accuracy within the well is required and lacks additional benefits outlined later in this paper.

Starting from governing equations typical of the petroleum industry, Cheng et al. (2005) present a boundary element method (BEM) numerical model that considers a finite-conductivity wellbore at arbitrary orientation. Wellbore conductivity, however, is calculated based on only two equations: one for laminar flow and a simplified, explicit equation for turbulent flow (from Brill and Mukherjee, 1999) representing all other flow

regimes. Although the BEM can sometimes be more computationally efficient than volume-discretization methods, it may lose this advantage as problems grow more complex and heterogeneous.

Semi-analytical solutions have been developed that couple all component mechanisms related to aquifer flow, pipe flow, orifice discharge and momentum exchange between radial inflow and main axial flow [Garg and Lal (1971); Cooley and Cunningham (1979)]. These solutions are based on two-dimensional, radial flow that precludes both aquifer heterogeneity and a solution to the less symmetrical problem of flow to a horizontal well. Many semi-analytical solutions for partially penetrating, arbitrarily inclined wells, such as that of Zhan and Zlotnik (2002), treat the well as a line source and impose on it a limiting assumption of either a uniform head or uniform flux. The semi-analytical approach by Tarshish (1992) avoids the assumption of either uniform head or uniform flux but presents a solution limited to steady-state flow in an aquifer of infinite lateral extent, overlain by a constant head reservoir, in which wellbore flow is strictly turbulent. Graber (2004, 2007) presents a more complete solution, accounting for most of the aforementioned energy loss mechanisms, but as the solution is derived for collection conduits surrounded by water, a constant head is assumed in the medium surrounding the conduit – an assumption that cannot usually be justified in groundwater hydrology modeling. The solution also presumes flow is always turbulent.

One of the most comprehensive treatments of this problem to date has been conducted by Lieuallen and Sawyer (1995, 1997) who modify the MODFLOW well package to avoid

making either of the limiting assumptions of uniform head or uniform flux along the well face. Their work incorporates flow between adjacent model cells that contain a well by simulating flow through the well cells as flow through a closed conduit pipe. A composite conductance is assigned to well cells based on weighted values of flow within the well conduit and flow around the conduit in the cell containing the conduit. There are, however, limitations to the published results, which yield artificially low conductance values for well cells away from the discharge cell. Also, Lieuallen and Sawyer (1995, 1997) account for only four of the five possible flow regimes.

The purpose of this research is to simulate flow in a porous medium penetrated by a finite length well, using the equations of flow in the aquifer coupled to flow along the axis of the well screen. To simulate wellbore flow, an equivalent hydraulic conductivity is assigned to each well cell/node based on in-well flow conditions related to pipe flow regimes and pipe friction. As there can be five possible flow regimes (laminar, critical, smooth, transitional or rough turbulent), an iterative process is performed to determine the appropriate equation governing pipe flow, as defined by the flow Reynolds number inside the well. The goal is not to create an entirely new, stand-alone model (such as that of Chen et al. (2003) or Cheng et al. (2005)), but to make use of existing numerical solvers, creating a more complete, versatile package. This was accomplished through the enhancement of two widely applied numerical models, MODFLOW, the U.S. Geological Survey's three-dimensional, finite-difference flow model, and *HydroGeoSphere*, a three-dimensional, finite-element/finite-difference, fully integrated surface-subsurface flow and transport model. This study also provides a suggested method for including the

remaining two hydraulic loss mechanisms, related to screen orifices and momentum exchange within the well.

Refining the flow treatment at the well screen should be especially beneficial for tracer and flowmeter tests, or wherever in-well hydraulics is important (Cassiani and Kabala, 1998; Halford, 2000). This usefulness is highlighted for such circumstances as quantifying aquifer heterogeneity, where Sudicky et al. (1995) show that groundwater flux distribution along a well screen is highly correlated to the local hydraulic conductivity of the well's surrounding porous medium. Similarly, this usefulness may translate into enhanced understanding of near-well solute transport and capture details for remediation scenarios, most especially for horizontal wells, given their longer well screens. Horizontal wells can intercept a larger planar area (Sawyer and Lieuallen-Dulum, 1998), and as a result they may be more efficient and cost effective than vertical wells in certain remediation scenarios (O'Neil et al, 1999). Horizontal wells can be placed parallel to broad, vertically thin contaminant plumes, vastly increasing the per-well zone of influence and capture, leading to increased recovery efficiency and shorter remediation times (USACE, 1996; Allouche et al., 1998). Finally, increased accuracy of hydraulic head and flux distribution along the well screen allows for more informed decisions to be made about optimizing screen (diameter, length and material) and pumping rate selection where inflow velocities, sustainability and well efficiencies are of concern (Korom et al., 2003).

Aquifer hydraulic conductivities (K_{aqf}) investigated in this study range from 10^{-3} m/s to 10^{-5} m/s, over which significant results were observed. It is possible, however, that results will be significantly impacted for a wider range of K_{aqf} .

2.2 Theoretical development

2.2.1 Problem statement

A simplified version of the equation governing three-dimensional, transient flow in an anisotropic medium near a point sink is represented by

$$S_s \frac{\partial h}{\partial t} - K_i \frac{\partial^2 h}{\partial x_i^2} - Q = 0 \quad (1)$$

subject to any no-flow, specified head or specified flux boundary conditions on all boundaries, where S_s is specific storage, h is hydraulic head, t is time, K_i is hydraulic conductivity, Q is the pumping rate and i represents the x , y and z directions.

Generally, flow inside a closed conduit is governed by the Darcy-Weisbach equation (arranged to fit the root finding form):

$$f_D \left(\frac{L}{D} \right) \frac{u^2}{2g} - h_L = 0 \quad (2)$$

where $u(l, t)$ is the average cross-sectional velocity of flow within the pipe, and is related to the Reynolds number (Re) through

$$\text{Re} = \frac{Du}{\nu} \quad (3)$$

where l represents the axial coordinate of the well, h_L is the hydraulic head loss due to friction between well nodes separated by a distance L , D is well diameter, f_D is the Darcy friction factor, ν is kinematic viscosity and g is earth's gravitational acceleration.

By treating the wellbore as a porous medium with a variable hydraulic conductivity, equation (1) can also be applied to flow within the well where K_i is replaced by K_w , the hydraulic conductivity within the well and along its axis. By recognizing that the fluid flux, q_w , along the well is equivalent to u , combining equations (2) and (3) yields

$$q_w = -\frac{2gD^2}{\nu \text{Re} f_D} \frac{h_L}{L} \quad (4)$$

Given that the Darcy equation for fluid flux at any point in a porous medium is

$$q_i = -K_i \frac{\partial h}{\partial x_i} \quad (5)$$

(4) and (5) are equated to give

$$K_w = \frac{2gD^2}{\nu \text{Re} f_D} \quad (6)$$

where $h_L \approx \partial h$ and $L \approx \partial l = \partial x_i$. These equations are derived by making the following assumptions regarding the various energy loss mechanisms: 1) frictional losses between the fluid and the inner well screen wall are both significant and related to a variable Re ; and 2) momentum exchange (as fluid enters the well screen radially, turns to flow axially and accelerates along the wellbore) and orifice discharge are insignificant.

In order to properly couple aquifer hydraulics and flow in the well in a numerical model, pipe flow hydraulics must be considered. This can be accomplished by treating the well

as an integrated portion of a porous medium and assigning aquifer-equivalent properties such as hydraulic conductivity. When calculating well conductivity (K_w), the flow regime and corresponding Reynolds number, and the Darcy friction factor must be determined. These variables are in turn dependant on hydraulic head values of adjacent well nodes (or cells), and so an iterative process is required to calculate values for h , based on K_w , and f_D , which are in turn based on h . In this way, neither a uniform flux nor a uniform head is assumed along the wellbore. Discharge is assigned to a single node (or cell), and head within the well is calculated as in the aquifer, using an equivalent conductivity (or conductance) for each well node (or cell).

In the numerical simulations considered, the values h_L , L , D , ν and g should be known, while the values of u , Re and f_D must be determined such that they satisfy (2) and (3). A third equation is therefore necessary to solve for these three values and is described in the following section.

2.2.2 Pipe flow

It is commonly accepted that fluid flowing in a pipe at low Reynolds number is steady and viscous (i.e. laminar) or unsteady and churning (i.e. turbulent) at high Reynolds number. For Reynolds numbers between these two extremes, flow is termed transitional and is a mixture of laminar and turbulent flows. The familiar Moody diagram (Moody, 1944) divides pipe flow into four distinct zones: the laminar, smooth turbulent, transitional turbulent and rough turbulent regimes. The short gap in the curves between laminar and smooth flow is the critical regime, where flow transitions in a sharp and unspecified manner. The equations that follow have been selected to define each of the

four well-defined flow regimes, with an additional equation defined for the critical flow regime.

Absolute boundaries between flow regimes do not exist, and there are no universally accepted values of Reynolds number at which flow transitions from one regime to another. Different sources quote different values. Additionally, the range in Re can be dependent on the form of the equation chosen. For example, some equations define Re explicitly in terms of the friction factor, f_D , while others are more complex and define it implicitly. Nevertheless, in the following, the sources from which Re values have been selected are cited with each corresponding equation.

Laminar flow is commonly described by the Hagen-Poiseuille equation

$$f_D = \frac{64}{\text{Re}} \quad (7)$$

for $0 < \text{Re} \leq 2000$. Upper limits vary between Re values of 2000 and 3000 from source to source, but larger values are often adopted where fewer flow regimes are considered. A value of 2000 is selected following the approaches used by Brill and Mukherjee (1999) and Kreith (2005).

For *critical flow*, experiments have shown that the relationship between f_D and Re is not well behaved and no precise equation exists for this regime. Following Schroeder (2001), a linear relationship is assumed by connecting endpoints of the two neighbouring flow regimes, laminar and smooth turbulent. The relationship, derived here, is of the form

$$f_D = m \text{Re} + b \quad (8)$$

for $2000 < \text{Re} \leq 3250$ (selected from Schroeder, 2001, though published upper limits vary between 3000 and 4000), where

$$m = \frac{f_{D_c} - 64/2000}{3250 - 2000} \quad (9)$$

$$b = 64/2000 - 2000m \quad (10)$$

and $f_{D_c} \equiv$ Darcy friction factor as calculated at the lower limit of the smooth turbulent regime (which equals 0.042515 at $\text{Re}=3250$ from (11) and supported by Nikuradse data). Alternatively, this value of f_{D_c} could be selected as the pipe-dependent lower limit of the transitional regime equation, for cases where flow bypasses the smooth regime and goes directly from critical to transitional flow. Because flow is so ill-defined in this regime, however, solution is somewhat arbitrary and for the sake of convenience the former alternative is selected.

Unfortunately some discontinuity in the $\text{Re}-f_D$ relationship cannot be avoided where pipe flow is considered. Discontinuity can arise in two places: 1) where flow develops from critical to smooth or transitional turbulent flow; and 2) where flow develops from smooth to transitional turbulent. There exist simplified, explicit equations describing the entire turbulent regime that can be used to sidestep the second of these two discontinuities. The first, however, is inevitable, as flow must somehow develop from either laminar or critical flow into turbulent flow. Introducing a critical equation, which has not been done yet for a groundwater application, avoids the sharper, discontinuous jump in f_D that will otherwise occur between the representative equations for flow in the laminar and

transitional regimes. The discontinuity is eliminated altogether where flow were to otherwise develop into smooth directly from laminar. In either case the model predicts experimental results more closely (e.g. Nikuradse, 1933) and reduces the likelihood of numerical instability.

Smooth turbulent flow can be described by a form of the Prandtl or Nikuradse equation

$$\frac{1}{\sqrt{f_D}} = 2 \log(\text{Re} \sqrt{f_D}) - 0.2 \quad (11)$$

for $3250 < \text{Re} < 6\sqrt{2}(D/e)/\sqrt{f_D}$ (Kutz, 1998). Equation (11), combined with the upper limit for Re in this regime, yields an explicit upper limit for the smooth regime (and lower limit for transitional) of:

$$\text{Re}_s = 3\sqrt{2} \left(\frac{D}{e} \right) \left\{ 4 \log \left[3\sqrt{2} \left(\frac{D}{e} \right) \right] - 0.4 \right\} \quad (12)$$

Transitional turbulent flow is best described by the implicit Colebrook-White equation (More, 2006), which is also used in creating the extensively used Moody friction-factor diagram. There are many popular, equivalent forms of this equation. Following Lieuallen and Sawyer (1995), transitional flow can be described by (Colebrook, 1939)

$$\frac{1}{\sqrt{f_D}} = 1.14 + 2 \log \left(\frac{D}{e} \right) - 2 \log \left(9.34 \frac{D/e}{\text{Re} \sqrt{f_D}} + 1 \right) \quad (13)$$

for

$$\frac{1}{120\sqrt{2}} < \frac{D/e}{\text{Re} \sqrt{f_D}} \leq \frac{1}{6\sqrt{2}} \quad (14)$$

where e is the absolute roughness of the pipe wall and e/D is referred to as relative roughness. Explicit alternatives to this equation also exist and perhaps the most accurate to date is presented by Sonnad and Goudar (2006). Given current computing power, the slightly more accurate implicit form can be adopted here without serious consequence.

According to Brill and Mukherjee (1999), *rough turbulent* flow is best described by one form of the Nikuradse equation for rough pipes

$$\frac{1}{\sqrt{f_D}} = 2 \log\left(\frac{D}{e}\right) + 1.14 \quad (15)$$

for $Re \geq 120\sqrt{2}(D/e)/\sqrt{f_D}$. Equation (15), combined with this lower limit for Re in this regime, yields an explicit lower limit for the rough regime (and upper limit for transitional) of

$$Re_R = 60\sqrt{2}\left(\frac{D}{e}\right) \left[4 \log\left(\frac{D}{e}\right) + 2.28 \right] \quad (16)$$

2.2.3 Numerical formulation

2.2.3.1 Pipe flow regimes

To solve for the friction factor in the well screen, a flow chart outlining the basic steps in selecting the appropriate third equation [i.e. (7), (8), (11), (13) or (15)] to use in addition to equations (2) and (3) is shown in Figure 3. In some cases, the bisectional root finding method is first employed to determine the type of flow and then to solve the above equations where f_D and Re cannot be explicitly resolved. If flow is determined to fall within either the smooth or transitional turbulent regimes, the equations that were solved in the Lieuallen and Sawyer (1995) algorithm implicitly, are in fact solved explicitly.

The root of equation (2) is designed to be the Reynolds number, when combined with equation (3) and one of the five regime equations. In employing the bisectional root finding method, an initial value of Re is selected to establish a first estimate of the root of the equation. Equation (2) is an increasing function and therefore the sign of the left hand side, designated f for convenience, will establish whether the true root of the equation is greater than or less than the estimated value; if f is negative the true root (Reynolds number) lies somewhere above the estimated root, and if f is positive the true root must be smaller than the estimated root.

To determine the flow regime, an implicit solution may be necessary because it is not known a priori which of the five flow-dependent equations is to be used. As indicated in Figure 3, the first estimated root of the algorithm is selected to be the upper limit of the laminar regime, $Re = 2000$, and the root finding function is completed using equation (7) for laminar flow. Where f is positive, the estimated Re is too large and flow falls within the laminar regime where Re can be solved for explicitly making use of the laminar flow equation (7). Similarly, a test for rough turbulent flow can be conducted using the lower limit for the rough regime (Re_R) established by (16) and the equation for rough flow, (15). Where f is negative, the estimated $Re=Re_R$ is too small and the true root must lie above the estimate, somewhere within the rough regime, which can then be solved for explicitly. If it is established that flow is neither laminar nor turbulent, an implicit solution is necessary to determine in which of the remaining three regimes flow now exists.

Firstly, a Reynolds number representing the upper limit of the smooth regime (Re_s) is determined by (12), where a value of $Re_s \leq 3250$ indicates that flow cannot be smooth (since this upper limit would represent a value that is smaller than the established lower limit for the smooth regime). Flow is therefore either critical or transitional. A $Re_s > 3250$ yields no new information and so a nested bisectional root finding function, g , is constructed from the smooth equation (11), rearranged to fit the root finding form in order to locate an f_D given Re_s . This inner root finding function will establish whether flow can be determined to be critical and smooth ($g \geq 0$) or critical and transitional ($g < 0$). To ensure the root of this solution is properly bracketed, starting lower and upper limits of f_D are selected as 0.001 and 1.0 respectively, based on extreme values of absolute roughness and pipe diameters for most real pipe data.

Next, an explicit expression is formulated for f_D by combining (2), (3) and (11) or (2), (3) and (13) depending on whether flow is critical or smooth, or critical or transitional. In either case, a corresponding Re value is then explicitly calculated using f_D along with the smooth (first case) or transitional (second) equations. Finally the flow regime can be specified by comparing the calculated value of Re to the upper limit of the critical regime ($Re = 3250$). In the first case, $Re > 3250$ indicates smooth flow, while $Re > 3250$ indicates transitional flow in the second case. Critical flow is established in either case for $Re \leq 3250$, in which case another step is required to calculate Re . To construct the linear equation of critical flow, (8), a second data point, f_{Dc} , is required for the upper limit of the interval. This point corresponds to the lower limit of the smooth regime,

calculated by the inner root finding function. Alternatively, as mentioned in section 2.2.2, this second point could be selected using the lower limit of the transitional equation if flow is determined to bypass smooth and go directly from critical to transitional. Finally, the critical flow equation (2), along with equations (2) and (3), must be solved implicitly, using the nested bisectional root finding method to determine a critical flow f_D and Re .

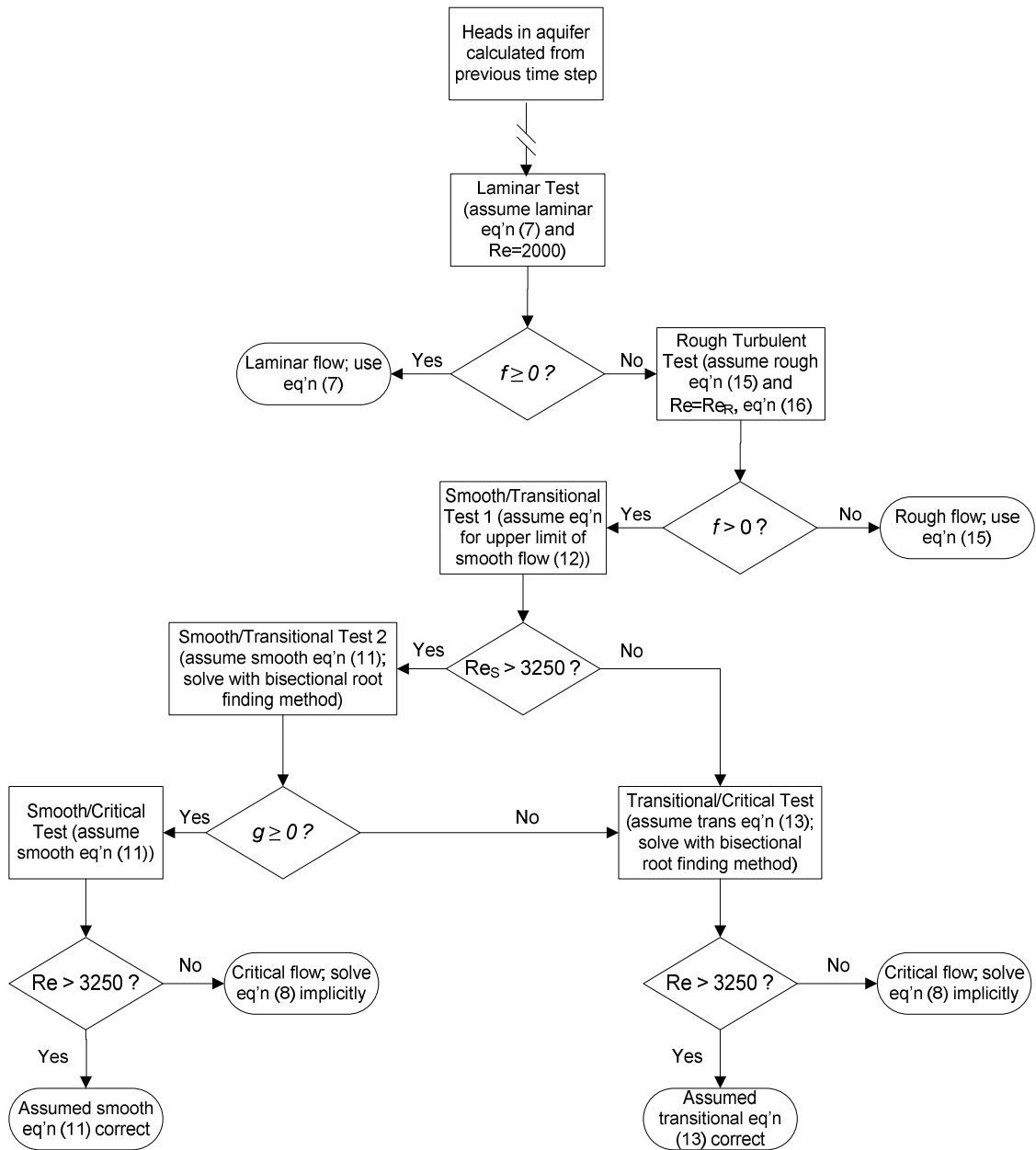


Figure 3 Flow chart for flow regime selection. f represents the bisectional root finding function of equation (2) to locate Re and g represents the nested bisectional root finding function to find f_D .

2.2.3.2 Numerical models

The major steps for implementing the procedure described above and for solving the hydraulic head distribution in a flow domain using *HydroGeoSphere (HGS)* are outlined

in Figure 4a. With hydraulic head values determined either from initial conditions or from a previous time step, the in-well flow conditions can be established. Re and f_D are then calculated, and the equivalent hydraulic conductivity (K_w) of each well segment (between two nodes) is then calculated. From the updated well conductivities, new hydraulic heads in the aquifer (and well) are calculated using the control volume finite element method. If the change in value of K_w for each well segment is not yet within tolerance criteria, new values of K_w are calculated based on updated head values and the rest of the loop is repeated. Once all K_w values have converged, the process either continues onto the next time step under transient conditions, or is terminated if steady state. An outline of the changes made to the *HGS* source code appears in Appendix I.

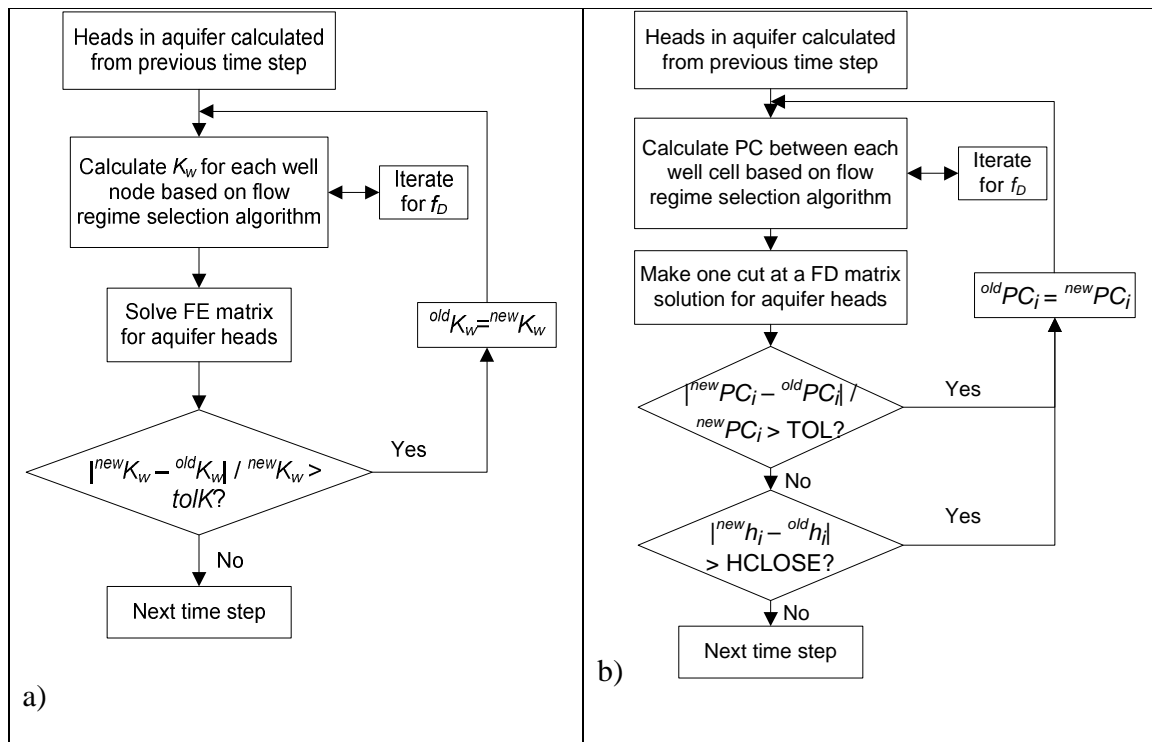


Figure 4 Flow chart for entire computational process in the modified versions of: a) *HydroGeoSphere* and b) *MODFLOW*.

Implementation of the overall computational process in MODFLOW (Figure 4b) is very similar to that in *HGS*, with the following exceptions. Once the flow regime is determined, an inter-cell conductance value analogous to equivalent hydraulic conductivity, PC (pseudo-conductance), is calculated between each adjacent well cell, because MODFLOW does not use hydraulic conductivity directly as in *HGS*. The value of PC is the weighted average of the well and surrounding medium conductances. One attempt is then made at approximating a solution to the system of finite difference equations. Closure criteria for both aquifer hydraulic heads and PCs are examined for each appropriate model cell, and the loop is repeated until convergence is obtained. An outline of the changes made to the MODFLOW source code appears in Appendix II.

2.3 Code Verification

Verification of the modified code is performed in three ways: 1) by comparing to the Theis solution; 2) by comparing to the original, unmodified code; and 3) by comparing to the results published by Chen et al. (2003), whose finite-difference model also accounts for wellbore frictional losses in a limited way (see Introduction). Prior to the comparisons, the model grid was tested and a discretization selected such that solutions were independent of nodal spacing and boundary effects during the pumping period. An additional note on grid discretization for the third comparison appears in section 2.4.1.

2.3.1 HydroGeoSphere

The first two comparisons are accomplished by modeling a pumping test in a confined aquifer, using the same model parameters selected for the grid verification (Table 1). The model domain is 10,000 m by 10,000 m in aerial extent, represented by 71 and 63 nodes

in the x and y dimensions, respectively, ranging in spacing from 0.1 m near the well to 1000 m near the outer boundary (see Appendix III for domain selection and grid verification). The additional nodes along the x-axis were inserted for observation well nodes. The domain is 300 m in thickness, represented by 31 evenly spaced vertical nodes. No-flow boundaries were selected for the upper and lower confines of the aquifer, while constant head conditions are imposed on all other outer boundaries. A uniform initial head is imposed on all aquifer nodes. The centrally-located, vertical pumping well fully penetrates the entire aquifer thickness.

Table 1 Aquifer properties used for model comparison between the Theis solution and the unmodified HGS code.

Parameter	Value	Units
Pumping rate (Q)	4.0×10^{-3}	m^3/s
Hydraulic conductivity (K)	2.3×10^{-5}	m/s
Aquifer thickness (b)	300	m
Specific storage (S_S)	7.5×10^{-4}	m^{-1}
Radial distance to observation point (r)	Variable	m
Screen diameter (D)	0.4	m
Absolute pipe roughness (e)	1.0×10^{-7}	m

Aquifer and well properties are chosen to allow the numerical model to resemble the simplified, analytical model as closely as possible; i.e. flow rates and pipe roughness are minimized while well diameter is maximized in order to eliminate frictional losses, and limit the hydraulic head gradient along the wellbore. A constant pumping rate of 345.6 m^3/day ($4 \times 10^{-3} \text{ m}^3/\text{s}$) is applied for a total simulation time of 116 days ($1 \times 10^7 \text{ s}$) and an adaptive time-stepping option is selected where the maximum allowed change in nodal hydraulic head between any time step is 0.5m (smaller values yield identical results). The large value of specific storage ($S_S = 7.5 \times 10^{-4} \text{ m}^{-1}$) was selected in order to minimize the effects of wellbore storage. HGS also provides a convenient method for eliminating

these effects (see Appendix IV for note on wellbore storage in *HGS*). Code verification, however, is independent of S_s .

A plot of drawdown versus time for three observation points is shown in Figure 5, the results of which are close to those obtained from the analytical solution. Drawdowns at the aquifer bottom will be slightly smaller than shown, given the non-ideal, non-uniform head condition along the wellbore of the numerical model. In the present simulation, however, this difference remains less than 0.001 m for the observation points shown. There are no boundary effects (i.e. 0% difference in drawdown between simulations with no-flow and constant head outer boundaries) in the time simulated, within 2250 m of the well.

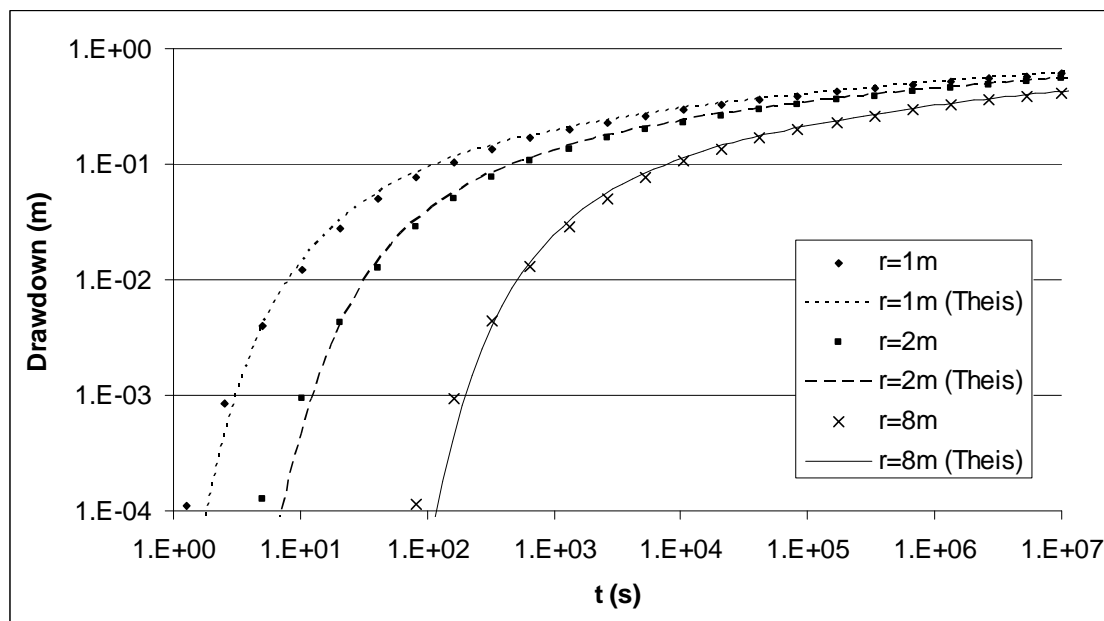


Figure 5 Drawdown at radial distances of 1, 2 and 8 m for pumping in a Theis aquifer. With a moderate pumping rate of $4 \times 10^{-3} \text{ m}^3/\text{s}$ (240 L/min) and a large well screen diameter ($D=0.4 \text{ m}$), frictional losses are minimized along the pipe and so flow within the wellbore remains close to laminar and the modified *HydroGeoSphere* solution matches closely the Theis solution. Data from the *HGS* solution is taken at the aquifer top.

Unlike MODFLOW, *HGS* already incorporates a finite conductivity wellbore, if only for laminar flow. This facilitates the comparison between the modified and original versions of *HGS*. Model parameters are chosen so as to limit wellbore flow to the laminar range (by selecting relatively small pumping rates and large screen diameters), under which circumstances the two models calculate similar values for K_w . By inspecting hydraulic head and flux distribution at each well node, it was observed that the maximum difference between the two solutions was less than 0.14 % for either variable, at $t = 10$ s, which dropped to less than 0.04 % at the end of the simulated time. The maximum difference always occurred at the pumping node. Similarly, the maximum difference between solutions for drawdown at radial distances beyond 0.5 m from the well, after $t = 10$ s, was 0.27 %. Differences between the two solutions at multiple observation points are listed in Table 2.

Table 2 Percent difference in drawdown between the modified and original versions of *HGS* for selected observation points. The maximum difference for each point is highlighted. r is the radial distance from the well node, which represents the center of the well, to the point of observed drawdown.

t (s)	% Difference at distance:					
	r = 0.5 m	r = 1 m	r = 2 m	r = 4 m	r = 16 m	r = 64 m
1.27	1.04	0.00	0.00	0.00	0.00	0.00
2.55	0.53	1.14	0.00	0.00	0.00	0.00
5.11	0.29	0.32	0.00	0.00	0.00	0.00
10.23	0.17	0.20	0.27	0.00	0.00	0.00
81.91	0.06	0.07	0.07	0.09	0.00	0.00
1311	0.04	0.04	0.04	0.04	0.02	0.00
2621	0.04	0.04	0.04	0.04	0.05	0.00
2.1E+04	0.03	0.03	0.03	0.03	0.03	0.02
1.0E+07	0.02	0.02	0.02	0.02	0.01	0.01

For the parameters selected, flow in the modified solution develops from laminar to smooth turbulent along the wellbore at any given time, while flow is always uniformly laminar in the original version. As wellbore flow in the modified model becomes more

turbulent (by decreasing well diameter, for example), the two models begin to slowly diverge, as expected. Likewise, if parameters are selected to produce more laminar flow in the modified version of the code, the difference between the two solutions goes to zero.

2.3.2 MODFLOW

The introduction of a finite conductivity wellbore into the USGS MODFLOW-2000 code is left unverified, but the changes made are essentially identical to those made in *HGS*. The importance of the proposed changes to the USGS code, however, could prove be of even greater value to MODFLOW, considering its current method of flux distribution along a well length. By default, MODFLOW assigns fixed values of flux per well cell by dividing well discharge in proportion to layer transmissivity, as follows:

$$\frac{Q_n}{Q_w} = \frac{T_n}{\sum T} \quad (17)$$

where Q_n is discharge to well in layer n , Q_w is total well discharge, T_n is the transmissivity of layer n and $\sum T$ is the sum of transmissivities of all layers penetrated by the well (McDonald and Harbaugh, 1988). This uniform, or specified, inner-boundary flux condition precludes any possible hydraulic head losses due to pipe friction, even for purely laminar flow.

No useful results will be obtained by modeling such a specified flux assumption using the newly modified code. It was observed, however, that the original and modified versions of MODFLOW yield equivalent results where a relatively uniform head can be simulated along the wellbore. To do this, an infinitely conductive wellbore was simulated in the

original model by assigning a series of contiguous model cells – representing the wellbore – with extremely high values of hydraulic conductivity. In the modified model, parameters were chosen so as to minimize hydraulic head loss along the wellbore, by selecting relatively small pumping rates (Q), large screen diameters (D), small pipe roughness (e), large aquifer conductivities (K_{aqf}), etc.

2.3.3 Comparison to the numerical model of Chen et al. (2003)

The aspects of the numerical formulation in the modified code particular to turbulent well flow are verified by comparing to results from the finite difference, aquifer-well coupled model by Chen et al. (2003). This model accounts for multiple flow regimes, including laminar, transitional and rough turbulent, in a horizontal wellbore pumped in a confined aquifer.

A rectangular domain was defined having dimensions of 116 m, by 3777.4 m, by 13.8 m in the x, y and z dimensions, respectively. A horizontal well of radius 0.025 m spans the entire length of the x-axis in the aquifer centre and is pumped from the x = 116 m end. The aquifer is homogeneous and isotropic with a hydraulic conductivity of 1.0 m/d (1.16×10^{-5} m/s) and specific storage of $1 \times 10^{-5} \text{ m}^{-1}$. All boundaries are no flow except for the aquifer top which is represented by a first type boundary condition, having a constant head of 10 m. Initial head throughout the aquifer is also set to 10 m. Instead of specifying a pumping rate, Chen et al. (2003) assigned a specified head at the pumping node. It was assumed that the specified head at the well exit was a linear interpolation between 0 m, at the start of the simulation, and 10 m at the end of the simulation.

The grid nodal spacing selected for this comparison matches that of Chen et al. (2003). A note on this grid and grid design in general follows in section 2.4.1. The x-axis, and well, is assigned 30 nodes and is divided into 29 uniform segments of 4 m each. The y-axis is non-uniformly assigned 25 nodes with grid steps ranging from 0.2 m near the well to 1000 m near the domain boundary. The z-axis is also non-uniformly assigned 15 nodes with grid steps ranging from 0.2 m to 2.0 m.

Given this model discretization, the two solutions agree (Figure 6, Figure 7 and Figure 8). Time step selection was also varied and appropriate values were selected. Absolute roughness of the well screen is 2×10^{-6} m, though this value is too small to significantly affect the solution.

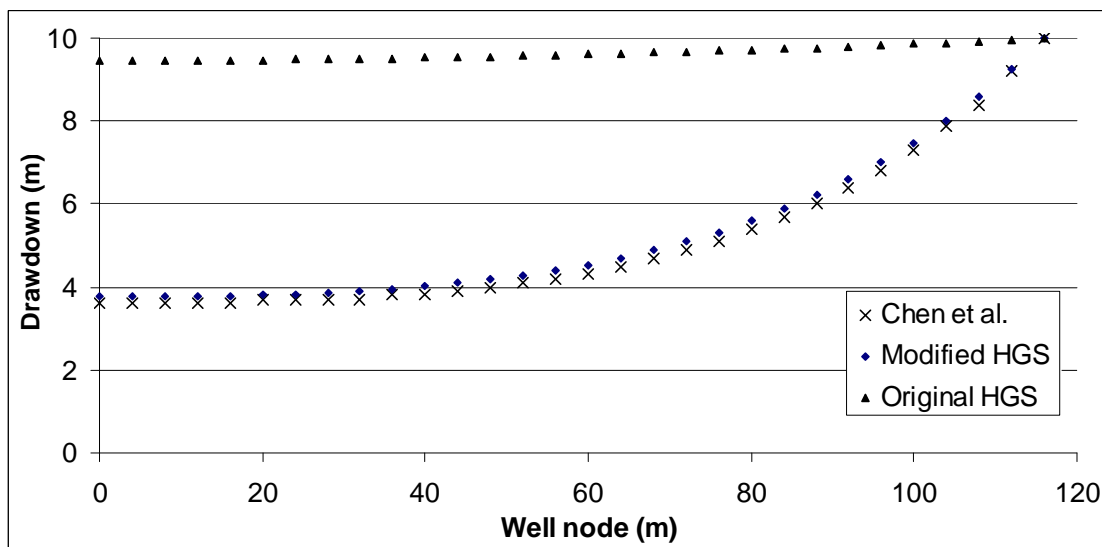


Figure 6 Comparison of the modified *HGS* solution and that of Chen et al. (2003) for drawdown distribution along a horizontal well screen. The data selected is from a published graph (fig. 2) and is accurate to within 0.1 m. The original, unmodified *HGS* solution is included for reference.

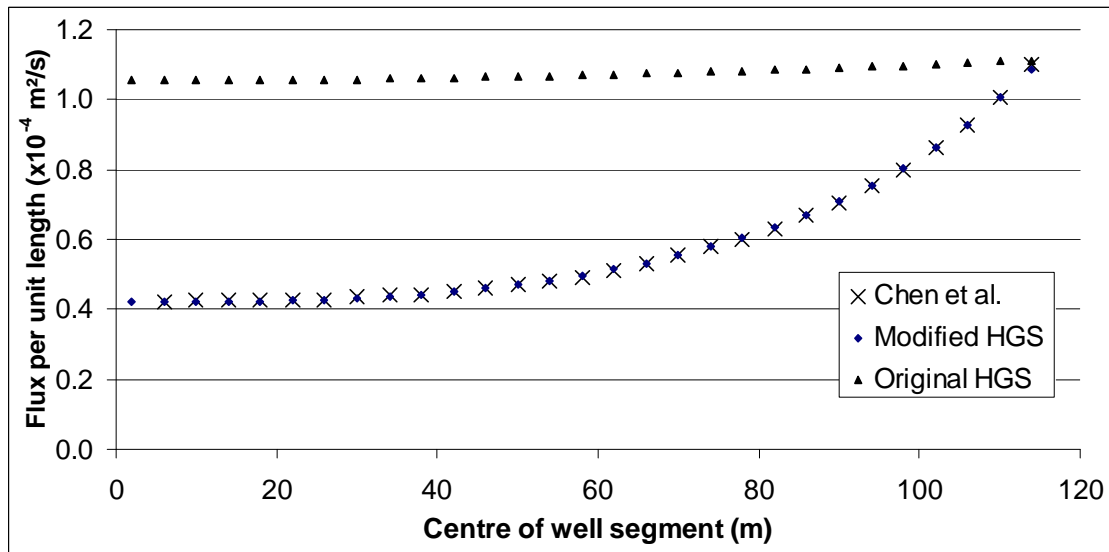


Figure 7 Comparison of the modified *HGS* solution and that of Chen et al. (2003) for well flux per unit length along a horizontal well screen. The data selected is from a published graph (fig. 3) and is accurate to within $1.7 \times 10^{-6} \text{ m}^2/\text{s}$. The original, unmodified *HGS* solution is included for reference.

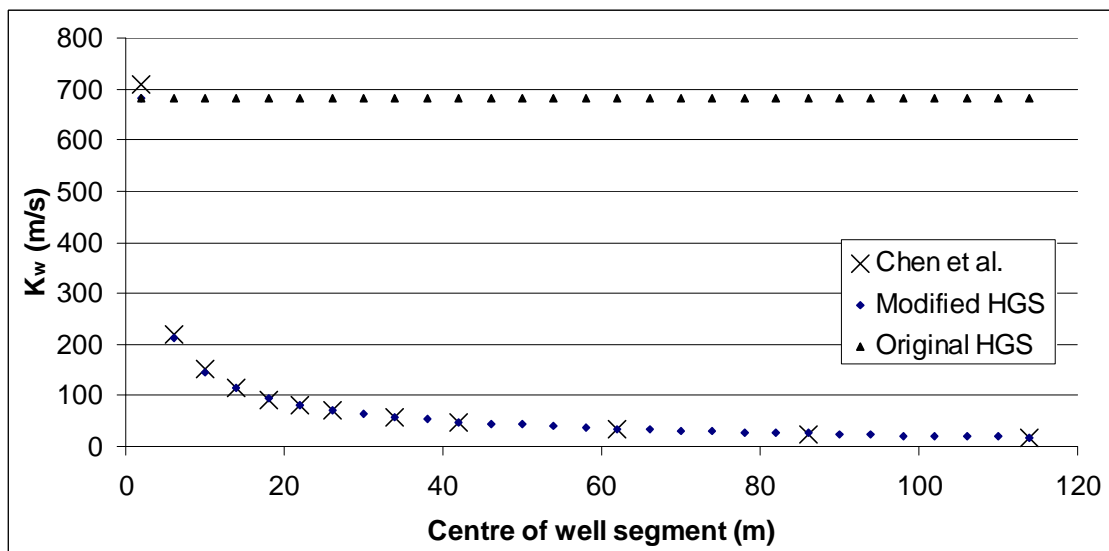


Figure 8 Comparison of the modified *HGS* solution and that of Chen et al. (2003) for well conductivity (K_w) distribution along a horizontal well screen. The data selected is from a published graph (fig. 4) and is accurate to within 12 m/s. The original, unmodified *HGS* solution is included for reference.

2.4 Results and discussion

2.4.1 Grid design

Well screen dimensions are commonly very small at the scale of many modeling problems and the size of nodal spacing within the immediate vicinity of the well is not particularly problematic. Where conditions within the well screen are of particular interest, special care needs to be taken during grid design. For a finite-element model, the best solution will be obtained where the location of aquifer grid nodes nearest a well node are placed at a distance equal to the well screen radius, neither closer nor farther from the well node. This was discovered using the procedure described below. Cartesian coordinates were used, although the same principles hold for radial coordinates.

Where aquifer nodes were placed inside the well screen, it was observed that no stable solution for hydraulic head could be obtained using the existing, available models, and neither could a stable solution be obtained for flux distribution along the well where aquifer nodes appeared outside the well radius. Hydraulic head (h_w) in fact will tend to negative infinity as nodal spacing (in a radial direction from the well axis) between a well node and the nearest aquifer node is made infinitesimally small. This occurs because the hydraulic gradient increases indefinitely as a point source or sink is approached. A real well, of course, is not a point sink and no such infinite gradient should exist. If instead, a coarser grid was selected where the aquifer nodes nearest a well node were placed outside the well radius, the solution would similarly be in error, yielding results that varied with nodal spacing. Flux distribution (q) along the well screen, on the other hand, became stable for all simulations run with either the modified or original *HydroGeoSphere* codes,

once nodal spacing was decreased to the point where the first aquifer node was placed at the well radius (r_w). The solution remained stable for smaller nodal spacing, indicating that nodal spacing less than r_w does not improve the result. It is thus deduced that the best solution is obtained where the nearest aquifer nodes coincide exactly with the well radius; any closer and no stable solution for h_w is possible and any farther, no stable solution for q is obtained. For grids with a large number of nodes this may be difficult, and so the telescopic mesh refinement technique might be employed. Note that nodal spacing in the aquifer was also varied but with the first aquifer node nearest the well node fixed at a distance of r_w , yielding comparatively negligible differences in both h_w and q between solutions, indicating that the placement of the first aquifer node was more crucial than the refinement of the grid discretization beyond that first node.

With this in mind, it is worth revisiting the results from Chen et al. (2003). Using a similar grid design as the authors, the results they obtain can also be derived using the modified code presented here, as demonstrated in section 2.3.3. Following the above suggestion whereby the nodal spacing in the vicinity of the well is refined, however, different results than those presented by Chen et al. (2003) are predicted using the modified *HGS* solution. Given that they used a coarse discretization near the well (the smallest grid step being 0.2 m, where the well diameter is only 0.05 m), it may be possible that their grid design is too coarse near the well to accurately predict highly sensitive values of hydraulic head within the well.

In a second example, Chen et al. (2003) compare numerical and physical model results. Given that their values of K and S_s are obtained via inverse modeling, the agreement that they obtain between numerical and experimental data could be attributed to arbitrarily varying the vertical hydraulic conductivity of the top portion of aquifer. It could be interesting to compare their model with the one proposed here using a grid discretization near the well as described above. It may be that agreement between the physical model and each of the numerical models is possible for different values of K and S_s .

2.4.2 Sensitivity analysis

Using the model configured for the Theis comparison in section 2.3.1, the following *HydroGeoSphere* simulations give an indication of the sensitivity of the solution to well screen diameter, D (Figure 9), pumping rate, Q (Figure 10) and aquifer hydraulic conductivity, K (Table 3). Data is presented for the simulated time $t = 1.34 \times 10^6$ s, at which the solution is still independent of boundary conditions for all parameter values within the selected ranges (i.e. the difference between drawdowns for solutions with no-flow and constant head boundary conditions is less than 1% within 50 m of the well for all combinations of Q and K). The values selected for D and Q represent the range of values reported in the studies discussed in the introduction. K values were chosen to represent good water bearing formations, typical of sand and silty sand aquifers (Freeze and Cherry, 1979).

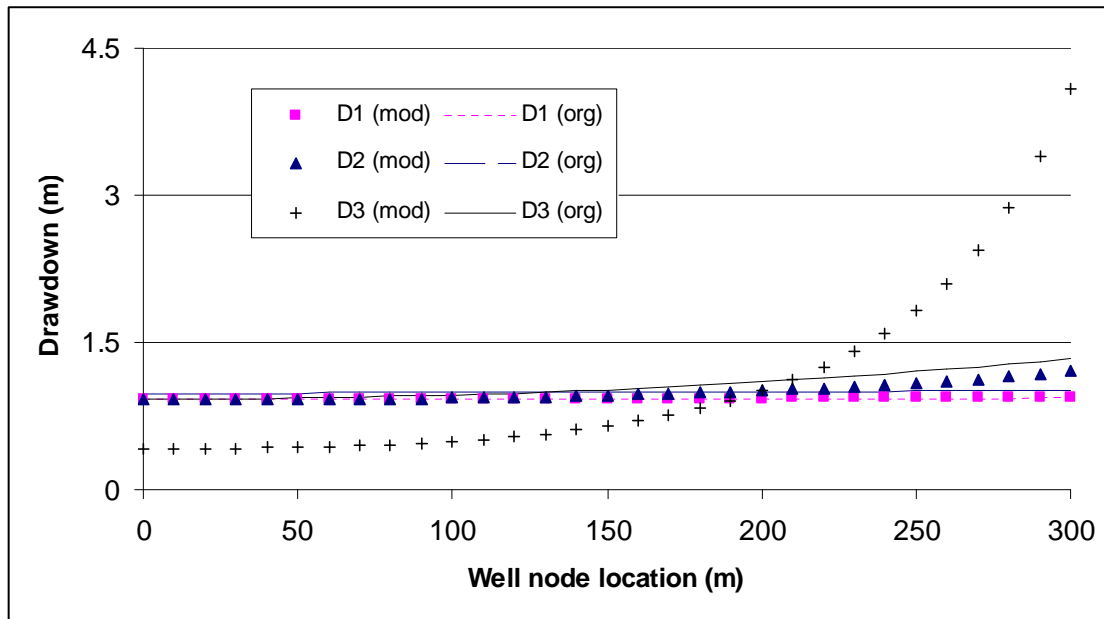


Figure 9 Drawdown along the well screen, indicating sensitivity of the modified *HGS* solution (mod) to screen diameter ($D_1 = 0.2$ m, $D_2 = 0.1$ m, $D_3 = 0.05$ m) for a pumping rate of 4×10^{-3} m³/s (240 L/min) and a negligible roughness, $e = 1 \times 10^{-7}$ m. The pump intake is located at node location 300 m. The results using the original code solution (org) are also presented for comparison.

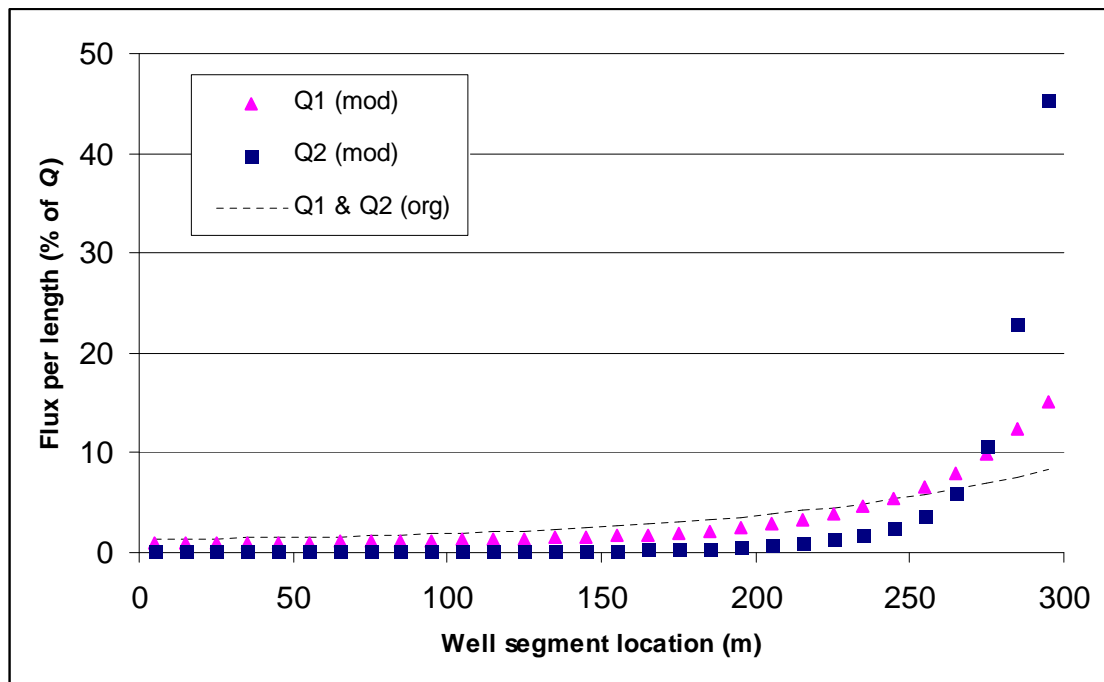


Figure 10 Flux per unit length of well screen, as a percentage of total pumping rate, Q , indicating sensitivity of the modified *HGS* solution (mod) to pumping rate, Q , for a screen diameter of 0.1m and a negligible absolute roughness, $e = 1 \times 10^{-7}$ m, for pumping rates $Q_1 = 1 \times 10^{-3}$ m³/s (60 L/min) and $Q_2 = 4 \times 10^{-2}$ m³/s (2400 L/min). The results using the original code solution (org) are also presented for comparison.

From Figure 9 it can be seen that as well diameter, D , is decreased, drawdown along the well screen increases near the pump intake, increasingly diverging from the classical prediction. In a similar trend, flux is also observed to increase along the wellbore, toward the pump intake, with decreasing D . Figure 10 reveals the increasingly asymmetrical solution for flux along the well screen, as pumping rate, Q , is increased. In a similar trend, drawdown is also observed to increase along the wellbore, toward the pump intake, with increasing Q . This trend is also reported by Mohamed and Rushton (2006) who indicate that the proportion of inflows from the aquifer to the well segments nearest the intake increase significantly with increasing Q . Analogous to pumping rate, the proportion of hydraulic head loss and flux near the pump intake are also observed to increase with an increasing pipe roughness, e , though results are less striking. Based on all simulations run in conjunction with the present study, it is estimated that values of $e < 1 \times 10^{-4}$ m will not impact the solution in any visibly discernible manner. If roughness values are expected to exceed an order of magnitude times this limit, which might be expected from heavily encrusted or rusty screens (ISO, 1991; Merritt, 1997), then e may begin to impact the solution depending on pipe diameter.

Pipe flow conditions, and the corresponding solution for head and flux within the pipe, will be most affected for scenarios where screen diameter is small and pipe roughness and pumping rate are large. Relative roughness (e/D) is also a relevant parameter, and in some cases where absolute roughness is large, e may have little influence where D is also large. Additionally, the most commonly used well screen materials, steel and PVC

(Sanders, 1998), have small values of absolute roughness [on the order of 10^{-5} m and 10^{-6} m respectively (Menon, 2005)] in which case e will have little to no effect on the solution. For aged or extremely rough pipe sections, roughness may become significant.

Table 3 Sensitivity of solution to aquifer hydraulic conductivity ($K_1 = 2.3 \times 10^{-5}$, $K_2 = 2.3 \times 10^{-4}$ and $K_3 = 2.3 \times 10^{-3}$ m/s): (a) percentage of flow entering the half of the well nearest the pump intake; and (b) hydraulic head loss (in meters) along the full length of the well screen. Pumping rate, Q , is 4×10^{-3} m³/s (240 L/min), well screen diameter, D , is 0.1m and absolute roughness, e , is a negligible 1×10^{-7} m at $t = 1.34 \times 10^6$ s. The solution using the original *HGS* code is also presented for comparison.

(a)				(b)			
	K1	K2	K3		K1	K2	K3
Modified	53.5	69.5	91.3	Modified	0.285	0.189	0.071
Original	50.4	53.6	73.2	Original	0.028	0.027	0.019

Aquifer hydraulic conductivity (K) can have the effect of pushing the solution toward the idealized limits of either a uniform hydraulic head with a highly non-uniform flux along the well screen for large values (K_3 in Table 3), or a uniform flux with a highly non-uniform head for small values (K_1 in Table 3). As K is decreased, flux per well node becomes increasingly uniform, while hydraulic head becomes increasingly non-uniform. The original version of *HGS* makes neither of these limiting assumptions, although by assuming only laminar flow in the wellbore its solutions tend to resemble more closely a uniform head condition, whereas the modified code will produce a spectrum of solutions within the range of these two extreme conditions.

Lengthening of the well screen will generally lead to lower drawdowns in the vicinity of the well. In long screen sections, however, hydraulic head loss from end to end may be significantly larger, making the well less effective at drawing water from sections distant from the pump intake. For example, doubling the length of well screen used in the simulation of section 2.4.4 [from Tarshish (1992)], from 22.3 m to 44.6 m, reduces the

total flux through the last 25 % of well screen from 8.5 % to 3.7 % of the total flux, for the short and long screens respectively.

2.4.3 Contour predictions

In addition to changes within the wellbore itself, a consequence of hydraulic losses along the well screen will be the change in head distribution within the aquifer. This can also impact the shape of capture zones and influence aquifer analysis. To investigate contour lines around a horizontal well, a rectangular-shaped, homogeneous, isotropic confined aquifer is selected. Aquifer thickness and initial head distribution are both uniformly 6 m. The model domain stretches between no-flow boundaries at $x = \pm 1300$ m and specified head ($h = 6$ m) boundaries along $y = \pm 350$ m. The 0.05 m diameter well is represented by 60 evenly spaced nodes and is centered within a horizontal cross-section of the model domain (Figure 11). The pump intake is located at $x = +150$ m and the well lies at a height of $z = 0.5$ m (above aquifer bottom), the elevation at which head contours are examined. The well is pumped for 10 days (8.64×10^5 s) at a rate of $240 \text{ m}^3/\text{day}$ ($2.78 \times 10^{-3} \text{ m}^3/\text{s}$). Aquifer conductivity is 5 m/day ($5.79 \times 10^{-5} \text{ m/s}$) and specific storage is $5 \times 10^{-4} \text{ m}^{-1}$.

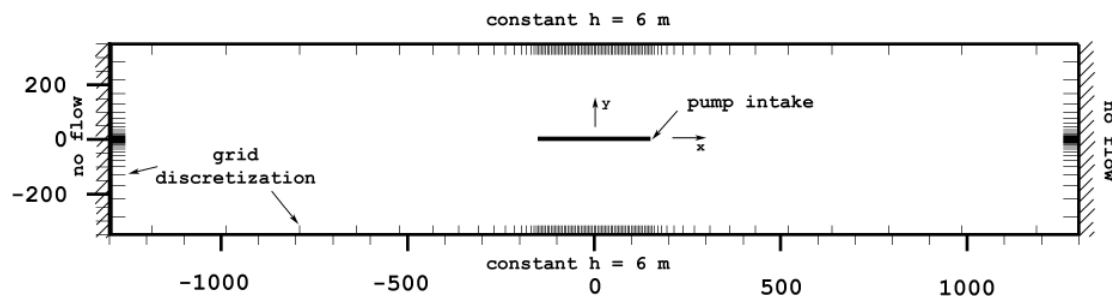


Figure 11 Plan view of domain used to investigate aquifer head contours. All figures in meters. Domain dimensions selected from model used in Mohamed and Rushton (2006), though grid discretization and some boundary conditions are different.

As observed by Lieuallen-Dulam and Sawyer (1997), hydraulic head contour lines are more asymmetrical and pear-shaped (Figure 12) than traditional solutions which assume either uniform flux or uniform head along the well screen (e.g. Figure 13). Given homogeneous and isotropic conditions, uniform flux models such as MODFLOW predict concentric, elliptical head contours centered on the middle of the well. Even the unmodified *HGS* code, which makes neither of the aforementioned assumptions, produces more symmetrical results (Figure 13). As can be seen in Figure 12, the modified code leads to steeper gradients in the vicinity of the pump intake location. Even at a perpendicular distance (along the y-axis) of 59 m from the well, drawdown in the modified solution remains significantly different: 30 % greater adjacent the well intake ($x = +150$ m), and 25 % smaller adjacent the well end ($x = -150$ m). Analogous contour patterns were observed for unconfined conditions (specific yield = 0.33).

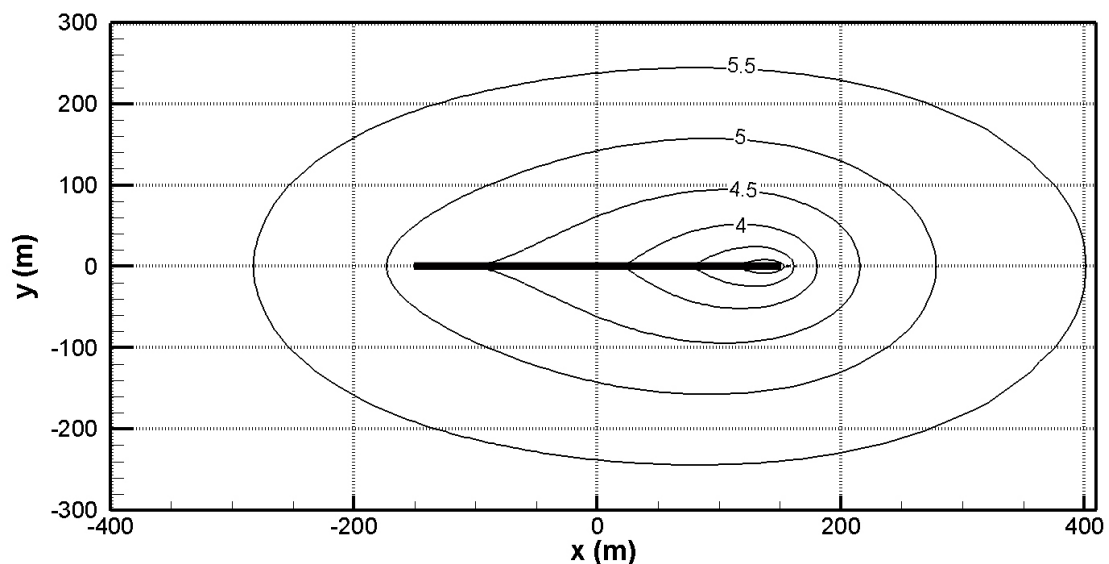


Figure 12 Highly asymmetrical hydraulic head contours generated using the modified version of *HGS* which includes well screen losses based on multiple flow regimes. The well screen is indicated by the horizontal line centered on location 0, 0. All figures in meters. Absolute roughness is equal to 8×10^{-4} m.

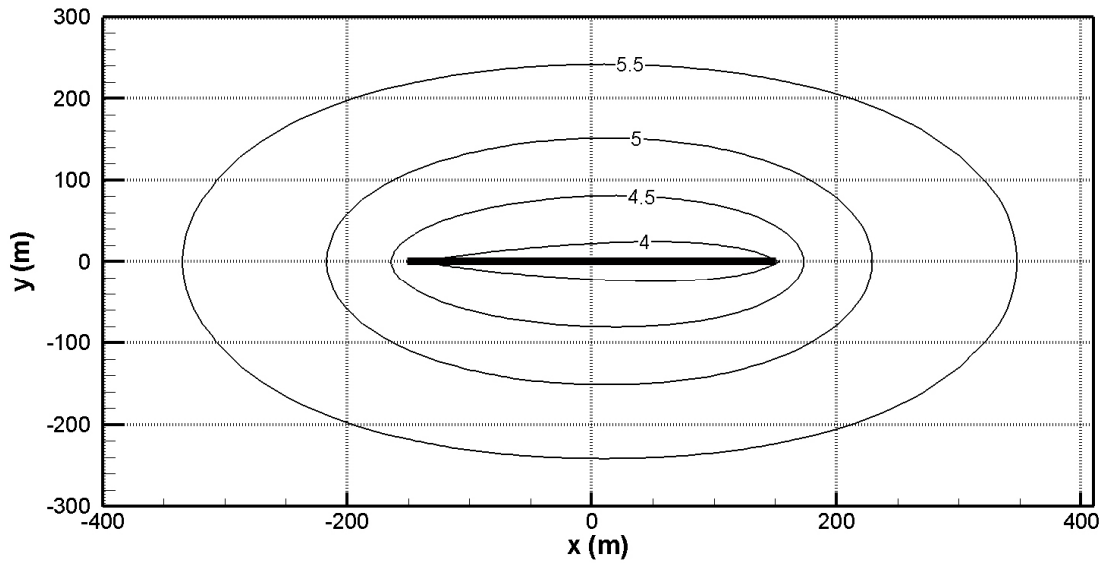


Figure 13 Hydraulic head contours generated using the original version of *HGS* which includes well screen losses based on laminar flow only. The well screen is indicated by the horizontal line centered on location 0, 0. All figures in meters.

Wellbore flow conditions, where Reynolds number increases toward the pumping node, are shown in Figure 14. The original *HGS* code assumes laminar flow throughout the wellbore and so K_w , equal to 58.9×10^6 m/day (682 m/s), is a constant throughout the simulation. Conversely, K_w is shown to decrease rapidly in the modified solution as flow begins to show signs of turbulence. Pipe flow in this simulation reaches four of the five flow regimes from rough turbulent at $x = +150$ m, to laminar at the well end.

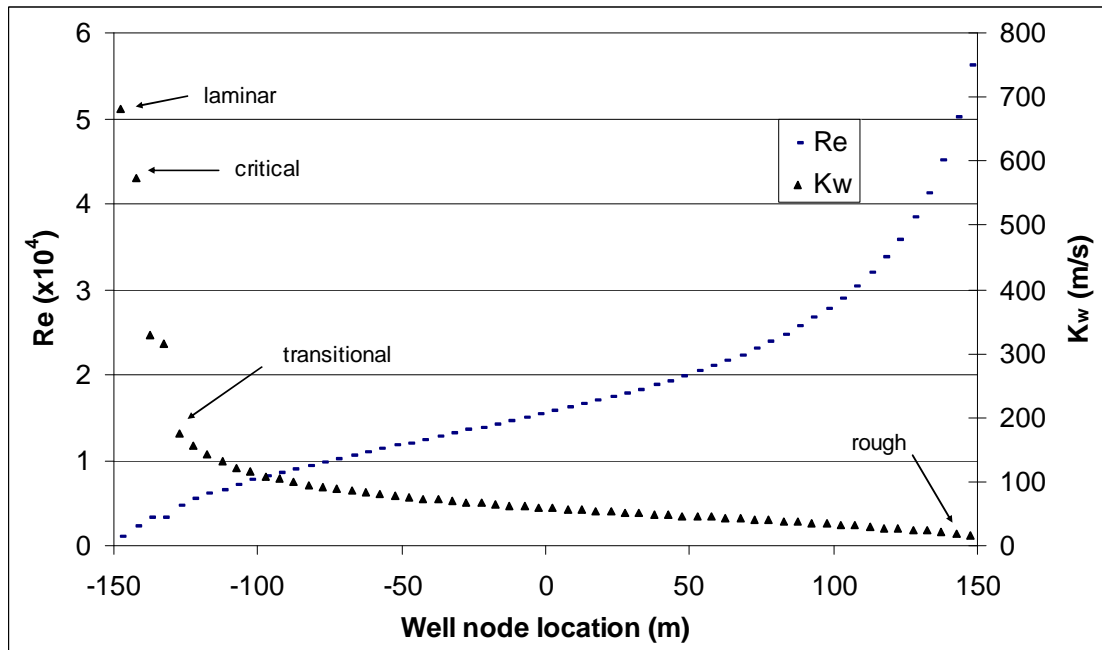


Figure 14 Reynolds number (Re) and hydraulic conductivity (K_w) at each well node along the wellbore generated with the modified *HGS* code for the contour prediction simulation. Flow regime labels point to the well segments in which the particular flow first appears while moving toward the pumping node, at node location +150 m.

2.4.4 Comparison to the semi-analytical model of Tarshish (1992)

The semi-analytical solution by Tarshish (1992) is limited to steady-state flow in an infinite, homogeneous, isotropic aquifer located under a water reservoir of constant head. It does, however, present a solution that includes frictional, orifice and momentum losses associated with well screen flow. A comparison of in-well hydraulic head and flux per unit length of well screen are compared against those generated by the modified *HGS* code in Figure 15 and Figure 16 respectively.

The modified *HGS* results (Modified *HGS* - 1) lie somewhere between the results from Tarshish and those generated with the original *HGS* solution (Original *HGS*). Flow within the well ($D = 0.15$ m) is smooth-turbulent using the modified model, while

Tarshish and the original solution assume a static flow that is strictly rough-turbulent and laminar, respectively. To determine whether the difference between the modified *HGS* and Tarshish models can be attributed to the different assumptions about flow regime selection or to the additional inclusion of momentum and orifice losses in the latter model, the *HGS* code was modified further such that frictional losses are calculated based strictly on rough-turbulent flow, where the Darcy friction factor, f_D , is assigned a constant value of 0.1 as does Tarshish. The results for this simulation (Modified *HGS* - 2) are closer to the Tarshish data, but it appears that hydraulic losses are still not quite as large. The same data set (Modified *HGS* - 2) can also be generated with the modified *HGS* code where absolute roughness, e , is set to 10^{-2} m, which is the value of e that roughly corresponds to $f_D = 0.1$ and $D = 0.15$ m from the Moody diagram.

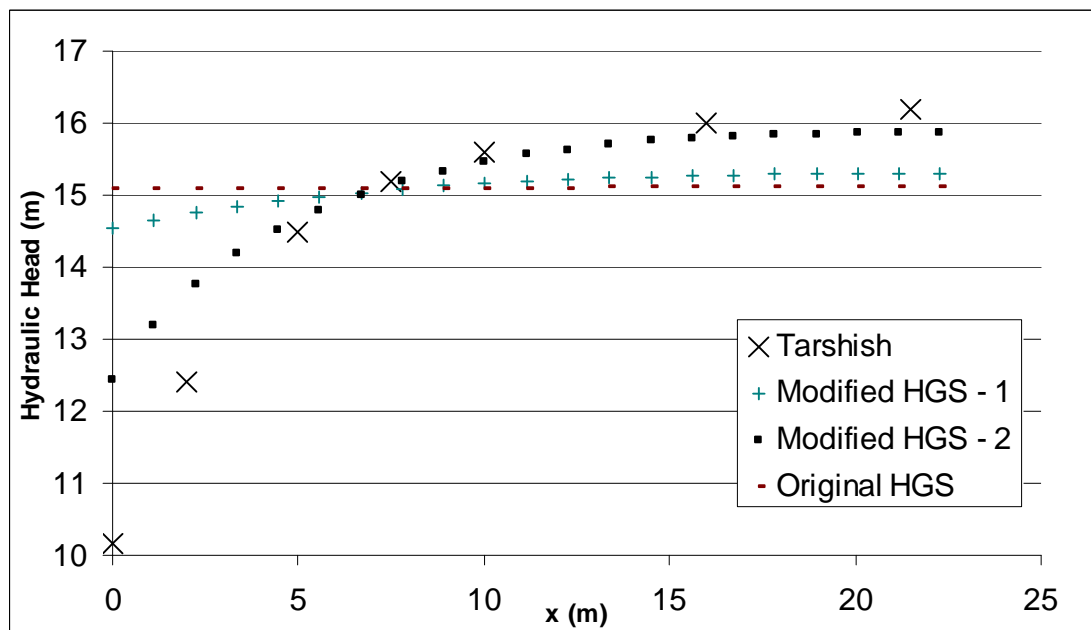


Figure 15 Hydraulic head along the well screen for the steady state simulation presented in Tarshish (1992), where water is pumped from $x = 0$. Results are presented from the original publication, along with the modified *HGS* solution (Modified *HGS* - 1) for a well diameter (D) of 0.15 m and a negligible value of absolute roughness ($e = 1 \times 10^{-8}$ m). *HGS* results produce flow that is smooth, while Tarshish assumes static turbulent flow. Modified *HGS* - 2 represents results where the code has been altered

to treat flow as strictly turbulent. Original, unmodified *HGS* results (Original *HGS*) are also presented for comparison.

The original, unmodified *HGS* solution (data set ‘Original *HGS*’ in Figure 15) generates a nearly uniform hydraulic head along the wellbore, where flow is assumed laminar at all times. The Tarshish model, on the other hand, leads to the largest drawdown of all solutions at the pumping node and the greatest head loss along the entire length of the well screen. The modified solutions fall somewhere between these two extremes. By comparing the Modified *HGS* - 1 and Modified *HGS* - 2 data sets, it is clear that frictional losses are overestimated by following Tarshish and assuming a static, rough-turbulent flow regime. From the Modified *HGS* - 2 and Tarshish data sets, it is clear that momentum and orifice losses do contribute to additional, significant hydraulic head loss. It should therefore be useful to incorporate these two additional loss mechanisms into the present solution. A practical method for doing this is proposed in section 2.5.2.

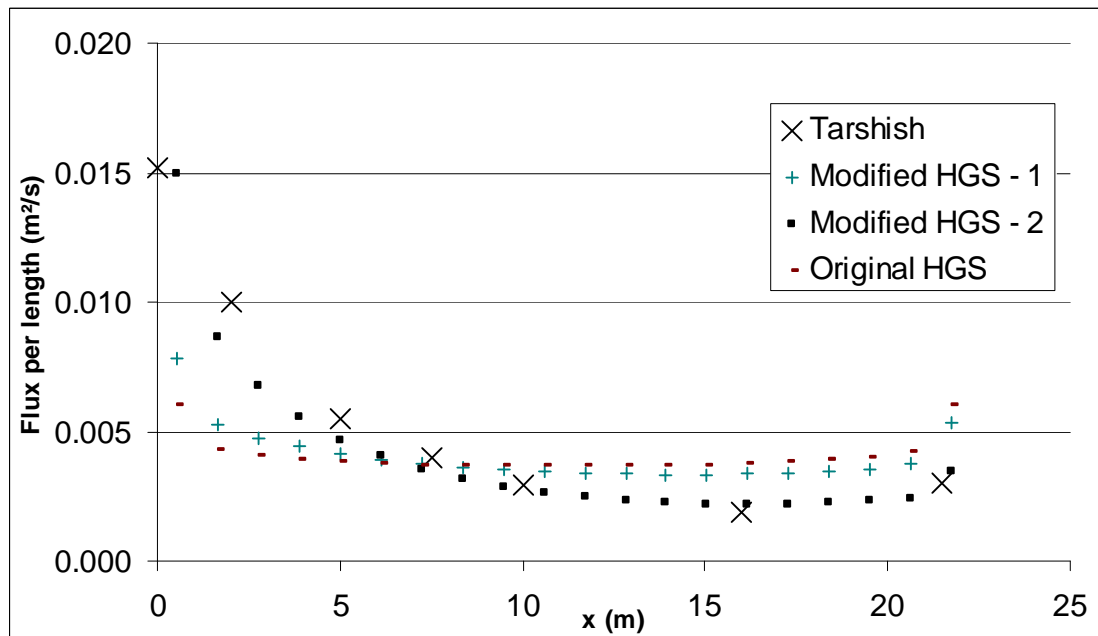


Figure 16 Flux per unit length of well screen. See Figure 15 for details.

2.5 Model limitations and future research

2.5.1 Limitations and suggested modifications

For honed surfaces of small relative roughness ($e_{rms}/D < 0.0025$), where an inflectional behaviour exists in the early transitionally rough regime similar to that observed in the sand grain roughness experiments of Nikuradse (1933), a slightly more accurate expression, derived by Allen et al. (2005), can be used in place of equation (13). It is not expected that this would have a large impact.

Well node desaturation can be a problem as both *HGS* and *MODFLOW* codes assume closed-conduit flow. For the case of a horizontal well in an unconfined aquifer where water level drops below the top of the well screen, there is no provision for converting to open-channel, or drain, flow. Additionally, because of the finite-difference approach in *MODFLOW*, this model should be used with caution where a horizontal well is constructed close to the water table. This is because if a modeling layer containing a well cell becomes only partially saturated, an error is introduced because of the unsaturated portion of the cell that is included in cell property calculations. Specifically, the cell's cross-sectional area perpendicular to flow, used in pseudo-conductance calculation, becomes smaller. As Lieuallen and Sawyer (1995) have determined, this error grows with the decrease in saturation percentage. The largest error will occur for the case where water level drops below the bottom of the well screen. In this case, a pseudo-conductance value for each affected well cell is still calculated although, practically, there should no longer be any flow through the empty well. If the cell dewateres completely,

however, no error arises because MODFLOW sets the dry cell's conductance (and pseudo-conductance) to zero and flow rate to or from this well cell is also set to zero. These limitations could be addressed by incorporating a well cell's saturation level, the elevation of the well relative to the water level and the wetted area of the pipe (Lieuallen and Sawyer, 1995). Because of the infinitesimal nature of the pipe diameter in the finite element calculations in *HGS*, there is no equivalent error associated with desaturation, and the well will either be 'on' or 'off'. Of course, as mentioned earlier, no open-channel flow is accommodated if the water table falls within the pipe itself. In this case tile drains should be used instead. An additional modification would be required in that similar frictional losses must be applied to tile drains.

As in all models that do not use the assumptions of prescribed head or flux along the wellbore, this model predicts higher fluxes in certain parts of the well, especially close to the pump intake. This may lead to non-laminar flow in regions outside the well, for which there is no accommodation in this model. Szekely (1992) acknowledges this possibility for long screens with high pumping rates by attempting to allow both a laminar and a turbulent flow in a skin zone surrounding the well screen.

Locating a pump intake within the well screen can increase well efficiency and decrease the differential entrance flow velocities along the screen length (VonHofe and Helweg, 1998; Korom et al., 2003). To upgrade to this type of system, friction factor calculations could be modified using expressions for flow between concentric annuli as presented in Brill and Mukherjee (1999).

Additional frictional losses due to pipe bends could also be included.

Absolute pipe roughness (e) is not a physically measured property, and as such, presents an inherent limitation. Moody (1944) produced results for several practical pipe materials and diameters to determine reasonable roughness values which are still accepted today (Brill and Mukherjee, 1999). Materials, however, can vary in nature as well as change over time from deposition and corrosion – though in extreme cases these behave more like diameter reduction – especially affecting flow in the transitional and rough turbulent regimes. It could therefore be desirable to accommodate pipes with varying or multiple values of e , as done in Szekely (1992) for screened and unscreened portions of a well. There is, however, a shortage of information on precise flow conditions relating to e (and f_D) for pipes with spatially varying inflow.

Inertia-induced oscillations of head response during hydraulic tests can lead to misleading estimation of hydraulic properties in highly permeable formations. Such behaviour is not considered here. For a mathematical model of groundwater flow in response to slug and pumping tests in high- K , confined and unconfined aquifers, the reader is directed to Butler and Zhan (2004) and Ostendorf et al. (2005), respectively. Both solutions, incidentally, incorporate a transient, laminar pipe friction, which the authors point out also contributes to underestimating K , especially for wells of small diameter.

There are five equations describing each flow regime within the well screen, and small discontinuities may arise between some of them. The possibility of solution oscillation (jumping between smooth and transitional flow, for example), leading to numerical instability, has been circumvented by placing a cap on the number of iterations allowed for well conductivity (K_w) calculations. The current maximum ($maxK = 20$) has been found to yield changes in values of K_w between final iterations that are acceptably small for all simulations. Errors in values of K_w translate into still smaller errors in values of influx and head within the well screen, and smaller still aquifer heads. The “*.73” ASCII output file can be used to monitor the iterative conductivity values, and should these values appear not to converge to within desired tolerance, the number of iterations can be increased. Alternatively, properties such as pipe roughness can be adjusted to obtain convergence.

It is perhaps worth trying to implement wells as 3D elements, instead of 1D line elements. This would allow the exact shape of the well to be modeled, reducing the amount of flow through the aquifer that should otherwise be flowing inside the well screen in the real world. When using line elements to represent the well screen, however, error will be minimized and likely negligible as long as the first aquifer nodes coincide with the well radius.

Lastly, experimental verification of the specific in-well hydraulics through tracer or flowmeter tests would be valuable.

2.5.2 Momentum exchange and orifice discharge

The work of Graber (2004) on submerged collection conduits surrounded by water could be modified to accommodate multiple flow regimes in the same way as has been done in this paper. An additional iterative loop could be inserted to determine a Darcy friction factor (f_D) based on the particular flow regime, instead of assuming a constant, turbulent value. The differential momentum equation for steady, spatially increasing, full-flowing conduits – equation (4) in Graber (2004) – can be used with a more general definition of f_D , which allows proper accounting for most major sources of hydraulic head loss: momentum exchange, screen orifice discharge and flow dependant friction.

In addition to this modification being especially beneficial for submerged conduits with large relative roughness values (e/D) and high flow rates, a solution to the problem of flow to a fully coupled well-porous medium system now becomes possible. Since the assumption of a constant head outside a well screen is not appropriate in most hydrogeological settings, the above modification to Graber's work alone is insufficient for the porous medium case. Combining the above model with the modified versions of MODFLOW or HGS described in this paper should make this possible. The aim would be to use the FD or FE matrix solutions for head, given relevant boundary conditions on prescribed aquifer nodes. A well could be represented as multiple constant head boundary conditions; values for which could be calculated using Graber's approach, making the following substitution: $\Delta\tilde{h} = h_a - h_w$ for $\Delta\tilde{h} = z - h$, and hence equation (15) in Graber (2004) would become

$$d(\Delta\tilde{h}) = dh_a - dh_w$$

where $\Delta\tilde{h}$ = head loss through well screen orifice, h = head in the water surrounding the conduit screen (a constant), z = depth of screen below water level, h_a = head at aquifer node (adjacent to well node) and h_w = head at well node. Instead of assuming a constant head (or head proportional to invert slope only) outside the conduit, a head of variable, but known (through the FD/FE solution) value, h_a , is assumed. The combined iteration scheme would look like: 1) assume initial head values h_a for the entire aquifer; 2) calculate values for $\Delta\tilde{h}$ and h_w using the Graber (2004) iteration technique (including the nested iteration for f_D); 3) assign model well nodes new h_w values; 4) regenerate the FD/FE matrix and solve for new values of h_a ; 5) repeat from step 2 until $|^{old}h_w - ^{new}h_w|$ is less than some tolerance criterion for each well node. Consult Graber (2007) for typographical correction to equation (16b) in Graber (2004).

2.6 Summary and conclusions

The solution presented in this paper provides a means of coupling the flow in an aquifer with flow in a pumped well, accounting for the variable conditions associated with pipe flow. This work extends the functionality of two existing software models, *HydroGeoSphere (HGS)* and MODFLOW, such that none of specified flux, uniform head and uniform pipe flow conditions need be assumed within and along the wellbore. Five flow regimes based on Reynolds number and Darcy friction factor are identified and incorporated, including critical flow which has previously been ignored in groundwater modeling research. The *HGS* version of the code was extensively tested and good agreement was found when compared to the analytical Theis model, the unmodified version of the *HGS* code and an existing numerical model that also considers the interaction between aquifer flow and flow within the wellbore.

Results confirm the finding of recent studies that both specified flux and uniform head along the wellbore are inappropriate assumptions for many applications. Results also indicate that the variable nature of flow within the well is significant. Where some mathematically coupled aquifer-wellbore solutions consider flow within the well to be static (e.g. strictly laminar or strictly rough-turbulent), all five flow regimes are considered separately here. The iterative steps for selecting the appropriate flow regime have been clearly outlined along with corresponding governing equations and their range of applicability.

Consequences of these findings include increased asymmetry of hydraulic head contours and steeper gradients in the vicinity of the pump intake than is classically predicted, particularly in high- K formations. This is a result of in-well hydraulic head loss being greatest near the pump intake. Factors contributing most to hydraulic losses include high pumping rate, small pipe diameter and large pipe roughness. Although a longer well screen may reduce drawdown in the vicinity of the intake, lengthening a well will also have the effect of increasing hydraulic head loss along its length, making the well less effective at drawing water from sections distant from the point of withdrawal. Application of this model could significantly impact the interpretation of wellbore flowmeter and tracer tests, improving the knowledge of aquifer hydraulic conductivity variation along the well screen. Pumping well system parameters such as well screen length, diameter, slot size and pumping rate can be more appropriately selected based on

refined contours, solute transport, capture zones, maximum specific discharge and efficiency and inflow velocity calculations.

Given that this model has been developed within multi-featured models, it provides the most versatile and general solution possible for any aquifer-well coupled solution. Significant features include fully three-dimensional geometry, arbitrary well inclination as well as packages that deal with surface-subsurface interaction and solute transport.

Results also indicate that although frictional losses may be the major source of hydraulic head loss in pipe flow, two other factors may play significant roles and should not be ignored: 1) orifice discharge, as flow enters through well screen slots; and 2) momentum change, as flow changes direction and accelerates as it enters the well and flows toward the intake. A practical method for including these sources of loss is described in the previous section, along with other suggestions for further refinement. With the noted exceptions in mind, the modified models presented here accurately represent head losses in the well for many practical situations.

A special grid design consideration for coupled models is also included, for simulations where hydraulic head within the well screen is of particular importance. For any model that treats the well as a sequence of point sinks, all aquifer grid nodes immediately adjacent to a well node should appear no farther and no closer than a distance equal to the well's radius.

2.7 References

- Allen, J. J., M. A. Shockling and A. J. Smits, 2005. Evaluation of a universal transitional resistance diagram for pipes with honed surfaces. *Physics of Fluids*, **17**, 121702.
- Allouche, E. N., S. T. Ariaratnam and K. W. Biggar, 1998. Environmental remediation using horizontal directional drilling: Applications and modeling. *Prac. Period. Hazard. Toxic Radioact. Waste Manage., ASCE*, **2**(3), 93-99.
- Brill, J. P. and H. Mukherjee, 1999. *Multiphase Flow in Wells*, SPE Monograph, Henry L. Dogherty Series, Vol. 17, Dallas, TX.
- Butler, J. J., Jr., and X. Zhan, 2004. Hydraulic test in highly permeable aquifers. *Water Resour. Res.*, **40**, W12402, doi:10.1029/2003WR002998.
- Cassiani, G., and Z. J. Kabala, 1998. Hydraulics of a partially penetrating well: solution to a mixed-type boundary value problem via dual integral equations. *J. of Hydrology*, **211**, 100-111.
- Chen, C. and J. J. Jiao, 1999. Numerical simulation of pumping test in a multilayer well with non-Darcian flow in the wellbore. *Ground Water*, **37**(3), 465-474.
- Chen C., J. Wan, and H. Zhan, 2003. Theoretical and experimental studies of coupled seepage-pipe flow to a horizontal well. *J. of Hydrology*, **281**, 159-171.
- Cheng, Y., D. A. McVay and W. J. Lee, 2005. BEM for 3D unsteady-state flow problems in porous media with a finite-conductivity horizontal wellbore. *Applied Numerical Mathematics*, **53**, 19-37.
- Colebrook, C. F., 1939. Turbulent flow in pipes with particular reference to the transitional region between smooth and rough wall laws. *J. Inst. Civ. Eng.*, **11**, 133.
- Cooley, R. L. and A. B. Cunningham, 1979. Consideration of total energy loss in theory of flow to wells. *J. of Hydrology*, **43**, 161-184.
- Freeze, R. A. and J. A. Cherry. 1979. *Groundwater*. Prentice-Hall, Inc., Englewood Cliffs, NJ.
- Garg, S. P. and J. Lal, 1971. Rational design of well screens. *J. Irrig. Drain. Div., Proc. Am. Soc. Civ. Eng.*, **97**(1), 131-147.
- Graber, S. D., 2004. Collection conduits including subsurface drains. *J. of Env. Eng., ASCE*, **130**(1), 67-80.

Graber, S. D., 2007. Full-flowing collection conduits with nonuniform inflow. *J. of Env. Eng., ASCE*, **133**(6), 575-580.

Halford, K. J., 2000. Simulation and interpretation of borehole flowmeter results under laminar and turbulent flow conditions. International Symposium on Borehole Geophysics for Minerals, Geotechnical, and Groundwater Applications, vol.7, pp.157-168.

Hantush, M. S., 1964. Hydraulics of wells. In: *Advances in hydroscience*. Academic Press, New York, NY.

Harbaugh, A. W., E. R. Banta, M. C. Hill and M. G. McDonald, 2000. MODFLOW-2000, The U.S. Geological Survey modular ground-water model – User guide to modularization concepts and the ground-water flow process. Open-File Report 00-92, U.S. Geological Survey.

International Organization of Standards (ISO 5167-1), 1991. Measurement of fluid flow by means of pressure differential devices, Part 1: Orifice plates, nozzles and Venturi tubes inserted in circular cross-section conduits running full. Reference number: ISO 5167-1:1991(E).

Korom, S. F., K. F. Bekker and O. J. Helweg, 2003. Influence of pump intake location on well efficiency. *J. Hydrologic Engrg., ASCE*, **8**(4), 197-203.

Kreith, F., 2005. *The CRC Handbook of Mechanical Engineering*. CRC Press, Boca Raton, FL.

Kutz, M., Ed., 1998. *Mechanical Engineering Handbook, 2nd Ed.* John Wiley & Sons, Inc., New York, NY.

Lieuallen, K. K., and C. S. Sawyer, 1995. Productivity comparison of horizontal and vertical remediation well scenarios using a connected well revision of a ground water flow model. *Tech. Completion Rep., Proj. No. G2009-12*, Univ. of Connecticut, Envir. Res. Inst., Storrs, Conn.

Lieuallen-Dulam, K. K., and C. S. Sawyer, 1997. Implementing intrawell, intercell flow into finite-difference ground-water flow model. *J. Hydrologic Engrg., ASCE*, **2**(3), 109-112.

McDonald, M. G. and A. W. Harbaugh, 1988. A modular three-dimensional finite-difference groundwater flow model. Techniques of Water Resources Investigations 06-A1, U.S. Geological Survey.

Menon, E. S., 2005. *Piping Calculations Manual*. McGraw-Hill Companies, Inc., New York, NY.

- Merritt, M. L., 1997. Computation of the time-varying flow rate from an artesian well in Central Dade County, Florida, by analytical and numerical simulation methods. U.S. Geological Survey Water-Supply Paper 2491.
- Mohamed, A. and K. Rushton, 2006. Horizontal wells in shallow aquifers: Field experiment and numerical model. *J. of Hydrology*, **329**, 98-109.
- Moody, L. F., 1944. Friction factors for pipe flow. *Transactions ASME*, **66**(8), 671-684.
- More, A. A., 2006. Analytical solutions for the Colebrook and White equation and for pressure drop in ideal gas flow in pipes. *Chemical Engineering Science* **61**, 5515–5519.
- Nikuradse, J., 1933. Laws of flow in rough pipes. *VDI-Forschungsh*, **361**, 1292.
- O’Neil, R. P., A. H. Smyth, J. May, and K. Preston, 1999. Horizontal vs. vertical wells; A comparison. *Water Well J.*, **53**, 34-40.
- Ostendorf, D. W., D. J. DeGroot, P. J. Dunaj, and J. Jakubowski, 2005. A closed form slug test theory for high permeability aquifers. *Ground Water*, **43**(1), 87-101.
- Park E. and H. Zhan, 2002. Hydraulics of a finite-diameter horizontal well with wellbore storage and skin effect. *Advances in Water Resources*, **25**, 389-400.
- Sanders, L. L., 1998. *A Manual of Field Hydrogeology*. Prentice Hall, Upper Saddle River, NJ.
- Sawyer, C. S., and K. K. Lieuallen-Dulam, 1998. Productivity comparison of horizontal and vertical ground water remediation well scenarios. *Ground Water*, **36**(1), 98-103.
- Schroeder, D. W. Jr., 2001. A tutorial on pipe flow equations. Unpublished. <<http://www.psig.org/papers/2000/0112.pdf>>
- Sonnad, J.R. and C. T. Goudar, 2006. Turbulent Flow Friction Factor Calculation Using a Mathematically Exact Alternative to the Colebrook-White Equation. *J. Hydraulic Engrg., ASCE*, **132**(8), 863-867.
- Sudicky, E. A., A. J. A. Unger and S. Lacombe, 1995. A noniterative technique for the direct implementation of well bore boundary conditions in three-dimensional heterogeneous formations. *Water Resour. Res.*, **31**(2), 411-415.
- Szekely, F., 1992. Pumping test data analysis in wells with multiple or long screens. *J. of Hydrology*, **132**, 137-156.
- Tarshish, M., 1992. Combined mathematical model of flow in an aquifer-horizontal well system. *Ground Water*, **30**(6), 931-935.

Therrien, R. and Sudicky, E. A., 2001. Well bore boundary conditions for variably saturated flow modeling. *Advances in Water Resources*, **24**, 195-201.

Therrien, R., R.G. McLaren, E.A. Sudicky and S.M. Panday, 2006. HydroGeoSphere: A Three-dimensional Numerical Model Describing Fully-integrated Subsurface and Surface Flow and Solute Transport, Manual (Draft), HydroGeoLogic Inc., Herndon, VA.

USACE, 1996. Horizontal directional drilling for environmental applications. ETL 1110-1-178. US Army Corps of Engineers. December 10, 1110-1178.

VonHofe, F. and O. J. Helweg, 1998. Modeling well hydrodynamics. *J. Hydraulic Engrg., ASCE*, **124**(12), 1198-1202.

Zhan, H., 1999. Analytical study of capture time to a horizontal well. *Journal of Hydrology*, **217**, 46-54.

Zhan, H., and V. A. Zlotnik, 2002. Groundwater flow to a horizontal or slanted well in an unconfined aquifer. *Water Resour. Res.*, **38**(7), 1108, doi:10.1029/2001WR000401.

Chapter 3 Summary and conclusions

The solution presented in this paper provides a means of coupling the flow in an aquifer with flow in a pumped well, accounting for the variable conditions associated with pipe flow. This work extends the functionality of two existing software models, *HydroGeoSphere (HGS)* and MODFLOW, such that none of specified flux, uniform head and uniform pipe flow conditions need be assumed within and along the wellbore. Five flow regimes based on Reynolds number and Darcy friction factor are identified and incorporated, including critical flow which has previously been ignored in groundwater modeling research. The *HGS* version of the code was extensively tested and good agreement was found when compared to the analytical Theis model, the unmodified version of the *HGS* code and an existing numerical model that also considers the interaction between aquifer flow and flow within the wellbore.

Results confirm the finding of recent studies that both specified flux and uniform head along the wellbore are inappropriate assumptions for many applications. Results also indicate that the variable nature of flow within the well is significant. Where some mathematically coupled aquifer-wellbore solutions consider flow within the well to be static (e.g. strictly laminar or strictly rough-turbulent), all five flow regimes are considered separately here. The iterative steps for selecting the appropriate flow regime have been clearly outlined along with corresponding governing equations and their range of applicability.

Consequences of these findings include increased asymmetry of hydraulic head contours and steeper gradients in the vicinity of the pump intake than is classically predicted, particularly in high- K formations. This is a result of in-well hydraulic head loss being greatest near the pump intake. Factors contributing most to hydraulic losses include high pumping rate, small pipe diameter and large pipe roughness. Although a longer well screen may reduce drawdown in the vicinity of the intake, lengthening a well will also have the effect of increasing hydraulic head loss along its length, making the well less effective at drawing water from sections distant from the point of withdrawal. Application of this model could significantly impact the interpretation of wellbore flowmeter and tracer tests, improving the knowledge of aquifer hydraulic conductivity variation along the well screen. Pumping well system parameters such as well screen length, diameter, slot size and pumping rate can be more appropriately selected based on refined contours, solute transport, capture zones, maximum specific discharge and efficiency and inflow velocity calculations.

Given that this model has been developed within multi-featured models, it provides the most versatile and general solution possible for any aquifer-well coupled solution. Significant features include fully three-dimensional geometry, arbitrary well inclination as well as packages that deal with surface-subsurface interaction and solute transport.

Results also indicate that although frictional losses may be the major source of hydraulic head loss in pipe flow, two other factors may play significant roles and should not be ignored: 1) orifice discharge, as flow enters through well screen slots; and 2) momentum

change, as flow changes direction and accelerates as it enters the well and flows toward the intake. A practical method for including these sources of loss is described in the previous section, along with other suggestions for further refinement. With the noted exceptions in mind, the modified models presented here accurately represent head losses in the well for many practical situations.

A special grid design consideration for coupled models is also included, for simulations where hydraulic head within the well screen is of particular importance. For any model that treats the well as a sequence of point sinks, all aquifer grid nodes immediately adjacent to a well node should appear no farther and no closer than a distance equal to the well's radius.

Appendix I: *HydroGeoSphere* modifications

The following is a list of all modified *HydroGeoSphere* files (build date version 20060626, local revision number 309), where all changes appear between corresponding “!MDC” comment lines:

1. hydrosphere.f90
 - bulk of code changes
 - subroutines affected: solve_flow, global_assembly_1d and newton_loop_flow
 - subroutines added: well_cond, well_flow_regime, bisect_smoothTrans, bisect_crit and computef
2. hs_mod.f90
 - added global variables: conwell_new(:), conwell_old(:), Kiter, maxK, K_converged, tolK, e_rough, max_delT and max_delT_iter.
3. init_final.f90
 - subroutine affected: read_hydrosphere_files
 - allocated space for arrays conwell_new(nwe) and conwell_old(nwe)
 - read e_rough from igen.

Files in need of additional modification to account for:

1. correct flow velocities:
 - linevel.f90: several subroutines
2. unsaturated flow where the well is other than horizontal:

- hydrosphere.f90, subroutines global_assembly_1d and well_cond, where total_head(i) [= hnew(node(i)) + elev(inloc(i))] should be substituted for hnew(i).

The following Grok files were modified to allow user input of absolute roughness (e):

1. segments.f90 (subroutine make_well) and
2. grok.f90 (subroutine write_hydrosphere_files).

File unit number 73 is used to output conwell-related data (K_w , f_D and Re) although no unit number reservation was made. If it is desirable to keep this output information, appropriate file handling might be added.

Note that subroutine assembly_element_1d (hydrosphere.f90) is called once more after the subroutine solve_flow (hydrosphere.f90) has solved the flow matrix (for entire problem if steady-state or time-step if transient). This means that well conductivities are calculated one additional time after they have already converged to within specified tolerance (from solve_flow) but will otherwise be accurate. If this is a nuisance for some reason, additional code modification can eliminate this final K_w recalculation.

The change to the input .grok file allows the user to input a value for absolute pipe roughness, e , read in as e_rough immediately following pipe radii in the input file (this is the only required change to the input). It should be noted, however, that code changes only affect wells created with the .grok command “make well” (i.e. “make well from

element list”, etc., are not affected). Currently there is only one value of e for all wells and an array of `e_rough` would be needed to account for well-specific roughness. In addition, pipe roughness is applied to well screen sections of pipe radius r_w only, and not to sections using a casing radius, r_c .

Note that the code will allow any value of well screen diameter (D) and absolute roughness (e) to be entered, although it should be understood that the pipe flow equations may not be defined for values of relative roughness, e/D , close to or greater than one, which can lead to erroneous results. The user must also ensure that absolute roughness is entered using the same units as declared in the `.grok` file.

Limitation to *HGS* code: if it is in fact possible to infill a horizontal well, the code currently assigns a value to K_w equivalent to the surrounding porous medium’s vertical hydraulic conductivity (`conwell=Kzz(zone_well(iwell))`), which means that if the horizontal well were to penetrate a vertical, low permeability barrier, flow would not be properly transmitted through the infilled wellbore as it might otherwise be if it were infilled with a material of higher permeability than it’s surrounding porous medium.

Convergence of well conductivity (K_w) is in part controlled by the tolerance level (`tolK`), which determines the fractional change allowed between successive K_w iterations for each well segment. Fractional changes from 10^{-5} to 10^{+3} were tested. For relatively constant model values (especially pumping rate) the solution sensitivity to `tolK` becomes negligible after early times, when flow becomes somewhat stable and changes in K_w

become reasonably small between time steps. A value of 10^{-3} is used in the code. A larger value, leading to slightly more efficient run time, could be implemented safely if very early time data is not critical and if pumping rates are not highly variable (i.e. on and off).

In order to preclude the possibility of solution oscillation, a cap on the number of iterations allowed for convergence of K_w within a single time step (*maxK*) has been set to 20. This value has been found to yield changes in values of K_w between final iterations which are acceptably small for all simulations. The “*.73” ASCII output file presents the largest fractional change in K_w at each time step, which can be viewed to ensure convergence. Otherwise, the number of iterations can be increased, *tolK* can be modified or properties such as pipe roughness can be tweaked to obtain convergence.

It is possible that further code modification is required for density-dependent flow and transport where the Picard linearization method is used.

Appendix II: MODFLOW-2000 modifications

The original work of Lieuallen and Sawyer (1995) was done in MODFLOW-88, while the current changes have been upgraded to MODFLOW-2000. Modifications have followed MODFLOW norms, making the program more modular than the original work, by bundling all changes into one new package, eliminating the need to modify unrelated packages (including the well package).

An implicit solution for f_D and Re has been replaced by an explicit solution once flow is known to fall within the transitional or the smooth regime. In addition to speeding up calculations, this eliminated the problem that the implicit bisectional root finding method had of not bracketing the roots of the transitional equation, which often returned Re values determined to be the lower limit of the search bracket (i.e. 2300). Part of this problem may have been due to the fact that the transitional equation is not well defined for small values of Re (near 2300) and the introduction of a critical flow equation has pushed the lower limit to a greater value (i.e. at least 3250, where flow bypasses the smooth regime).

Other significant changes to the code include correcting the misdimensioned SWAP array (in subroutine BNLISS) and the scaling of the earth's gravitational constant (in subroutine BNLI RP), the latter of which was causing highly inflated hydraulic losses near the pump intake. It is curious to note that in a follow-up paper by the same authors (Sawyer and Lieuallen-Dulam, 1998) that compares productivities of various horizontal and vertical remediation well scenarios, there is no reference to their earlier work that had included exactly such a study.

The only solver that was modified to make use of the new code was the SIP solver. Other solvers could also be modified easily, as the changes required are simple esthetic changes (i.e. related to output) and shouldn't require alteration for proper functionality.

An additional modification could be to make corrections to the calculated values of inter-cell conductance between well cells and vertically adjacent aquifer cells (variable VCONT).

Changes were made to three MODFLOW-2000 files (mf2k.f, sip5.f and utl6.f, though the latter two were only for esthetic, or output, reasons) and one new file (gwf1bnl2.f) was created for the introduction of the well loss package. Changes follow '!MDC' or 'cMDC' comment lines. The following input files require modification.

1. The following line must added to the name file:

```
Ftype      Nunit      Fname
```

where Ftype is designated 'BNL', and the Fname input file has a '.bnl' extension.

2. The Well input package follows the format in Harbaugh et al. (2000) with the following exceptions:

Append the text

```
AUX NCELLS AUX DIA AUX ROUGH
```

to input line number two (2. MXACTW IWELCB [Option]) where the new optional variables represent: the number of cells per well (NCELLS); the well screen diameter (DIA); and pipe absolute roughness (ROUGH). On line number six (6. Layer Row Column Q [xyz]), the above three variables can be input for each well. In contrast to the original input file, only the well cell coordinates corresponding to the pumping cell should be entered, along with the full pumping rate (Q) applied to that well. As in the original

file, input line number six should be repeated for as many wells as are entered on line 5.

The BNL (Bernoulli or well loss) package has the following format:

1. MXCELL

2. ITMP ILUNIT XLENG

3. Layer Row Column

(Item 3 is read for every well cell [including the pumping cell input in the Well package] of every well. Each cell of every well should be input contiguously, and each well's data input in the same consecutive order as input in the Well package. Item 3 is not read if ITMP does not correspond to ITMP in the Well package.)

MXCELL is the maximum number of cells contained within any of the wells;

ITMP is the number of wells and should equal ITMP of the Well package;

ILUNIT sets the input units (1 for meters and 2 for feet) and must correspond to the units selected in the GLO1BAS unit (read as LENUNI in the Discretization file);

XLENG is a multiplication factor for the unit indicated by ILUNIT (e.g. for units of km instead of meters, set ILUNIT to 1 and XLENG to 1000);

Layer is the layer number of the model cell that contains the well cell;

Row is the row number of the model cell that contains the well cell;

Column is the column number of the model cell that contains the well cell.

The input file requires a '.bnl' extension.

Appendix III: HydroGeoSphere grid verification

In order to verify the numerical formulation – through comparison with the analytical Theis solution – the *HGS* (unmodified code) model grid was selected based on the criteria that follow. An example from the *HGS* manual for code verification using the Theis solution was selected, using a (thicker) domain size of 10,000 by 10,000 by 300 m³ with a fully penetrating vertical well at $x = y = 5000$ m. A laterally extensive domain helps minimize outer boundary effects. The grid verification reported here was performed using the model design described in section 2.3.1, with the exception that $K = 2.3 \times 10^{-3}$ m/s, $D = 0.2$ m and simulation length was longer, although verification was also performed using the values of K and D listed in Table 1. Grid dimensions were varied with the following main results:

1. all grids more refined than 53 nodes in the x and y directions provide good agreement with the Theis solution (Figure 17), for observation well drawdowns at distances of 1 and 41 m from the pumping well (see also Figure 5);
2. the solution – for aquifer drawdown, and heads and fluxes in the well – is independent of outer boundary conditions prior to significantly large times (see below);
3. vertical discretization does not affect fluxes (Figure 18) or hydraulic heads (Figure 19) in the wellbore, and neither does it affect drawdown in the aquifer (Figure 20). 11 to 61 uniformly spaced vertical nodes were modeled;
4. horizontal discretization *does* affect heads and fluxes in the well. 20 to 121 nodes along each horizontal axis were modeled. Horizontal grid discretization g10 (53x53 nodes) was selected as the best choice, based on flux (Figure 21) and hydraulic head (Figure 22) values along the wellbore becoming relatively stable at

this point. Note that solution convergence is subject to the numerical model behaviour described in section 2.4.1 (Grid design) where nodal spacing near the well becomes small (i.e. where aquifer nodes appear within a well's radius of the well node).

To verify the effects of boundary conditions, both no-flow and constant head boundaries were modeled. Observation wells at 1, 55 and 2500 m confirm that aquifer hydraulic heads are consistent between models to within 3% at these distances for $t < 2.7 \times 10^6$ s, after which boundary effects begin to permeate the solution. At the largest tested pumping rate of $4 \times 10^{-2} \text{ m}^3/\text{s}$, drawdown within 40 m of the well differed by less than 1% at $t = 2 \times 10^6$ s between solutions with no-flow and constant head boundaries.

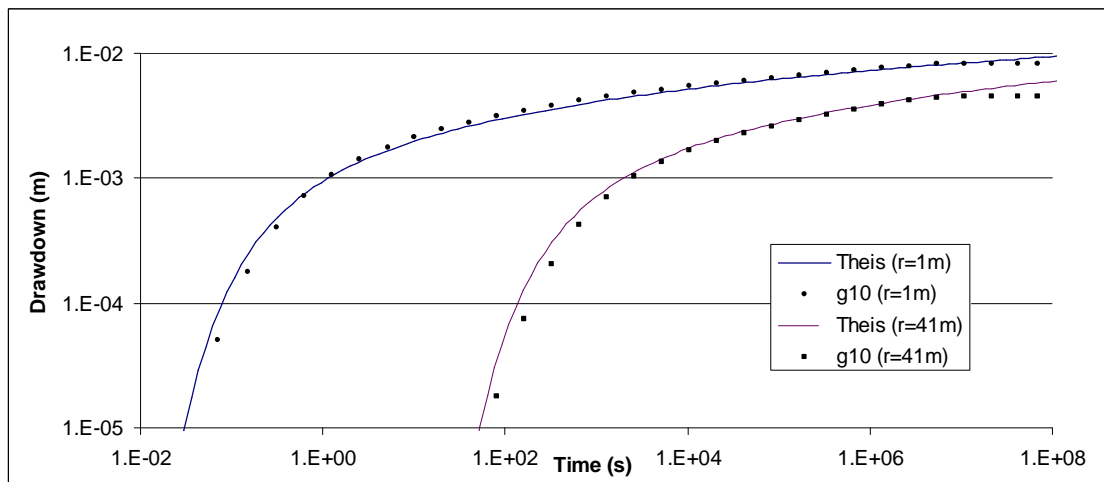


Figure 17 Drawdown at radial distances of 0.98225 m and 40.87747 m for pumping in a Theis aquifer. g10 corresponds to the *HGS* solution using a horizontal grid configuration of 53x53 nodes.

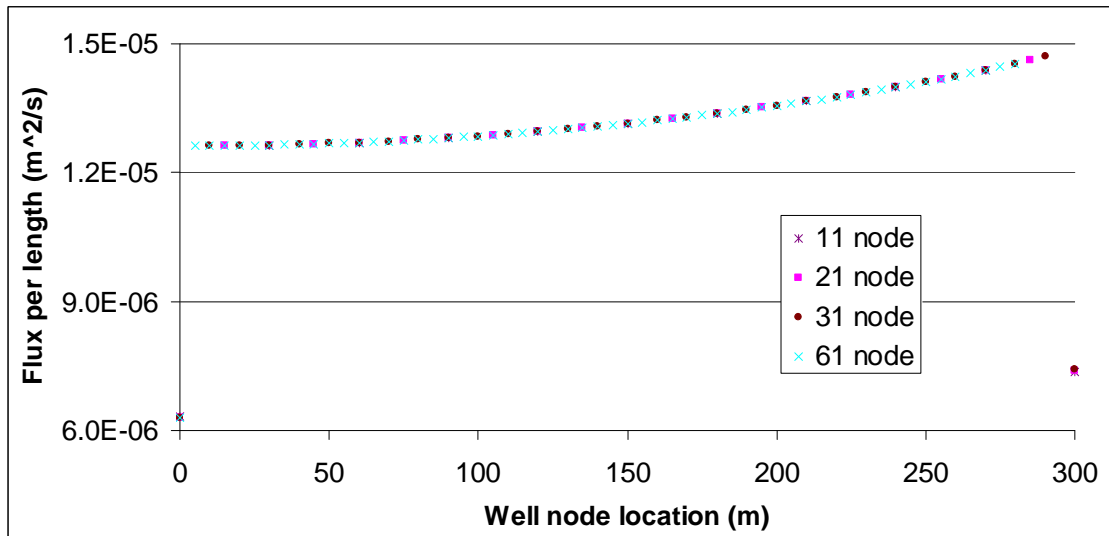


Figure 18 Flux per unit length of wellbore at $t = 42949672$ s, for vertical grid discretization of 11, 21, 31 and 61 nodes; g8 was used for horizontal discretization. No significant variation in flux is observed between grids for this and other times.

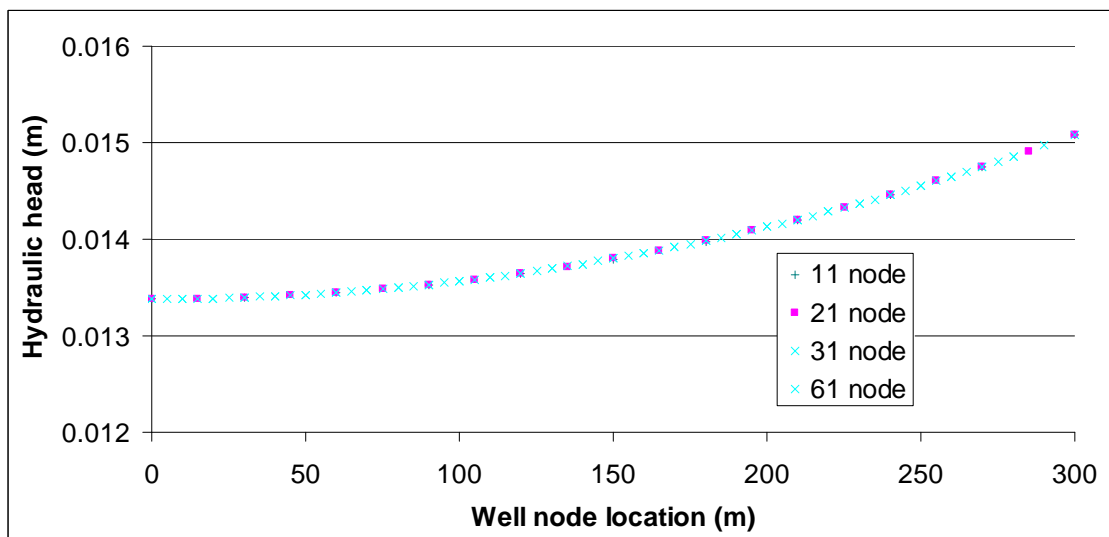


Figure 19 Hydraulic head along the wellbore at $t = 42949672$ s, for vertical grid discretization of 11, 21, 31 and 61 nodes; g8 was used for horizontal discretization. No significant variation in head is observed between grids for this and other times.

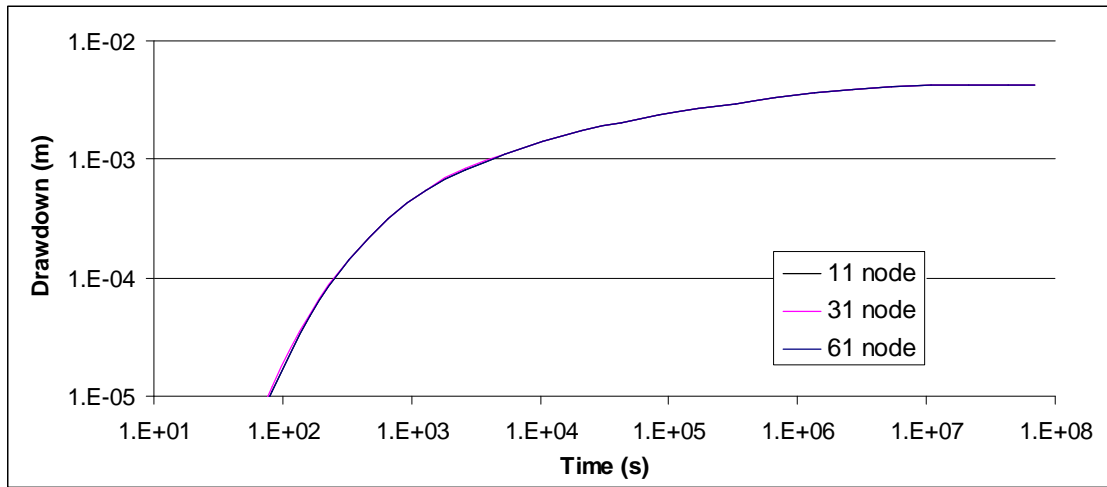


Figure 20 Drawdown at a radial distance of 52 m for pumping in a Theis aquifer using three different vertical node configurations.

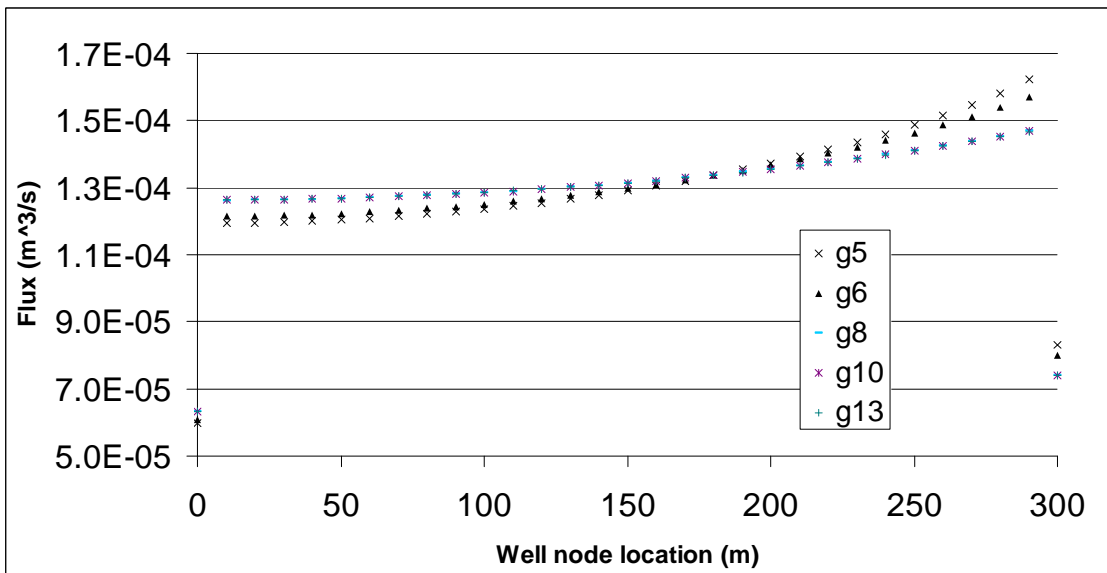


Figure 21 Flux per well node for various horizontal grid discretization at $t = 42949672$ s. The same pattern emerged at several simulation times.

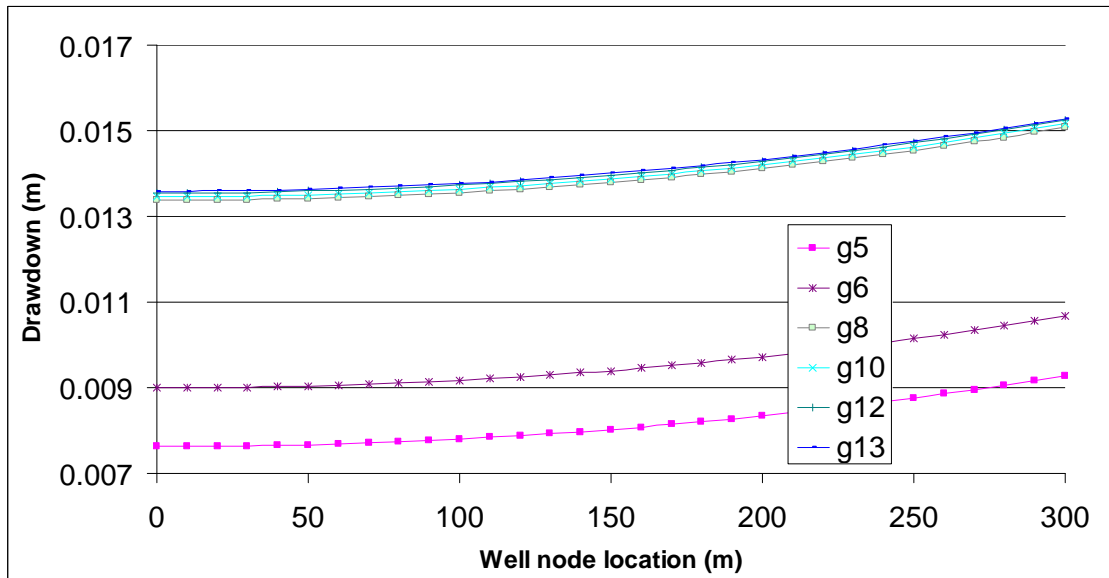


Figure 22 Drawdown within the well screen for various horizontal grid discretization at $t = 42949672$ s. The same pattern emerged at several simulation times.

Table 4 List of selected *HGS* grids tested with the Theis solution.

Grid name	Grid dimensions (x-y)	Smallest discretization (m)	Largest discretization (m)
g5	20-20	2.0	4500
g6	30-30	1.0	1500
g8	41-41	0.01	2394
g10	53-53	0.01	1000
g12	81-81	0.01	500
g13	121-121	0.01	400

For a verification of the original, unmodified *HGS* code, which accommodates a finite but static conductivity wellbore, see Sudicky et al. (1995) and Therrien et al. (2006).

Appendix IV: Note on wellbore storage in *HydroGeoSphere*

It is in fact possible to eliminate wellbore storage from *HydroGeoSphere* (*HGS*) calculations by setting r_c (caisson radius) to zero in the *.grok* input file. Regarding the code verification in section 2.3.1, it was observed that the modified *HGS* solution matched the analytical Theis solution more closely when wellbore storage was eliminated

in this manner (Figure 23). The value of specific storage (S_s) used to minimize the effects of wellbore storage was in fact unnecessarily high. Code verification is, however, independent of S_s .

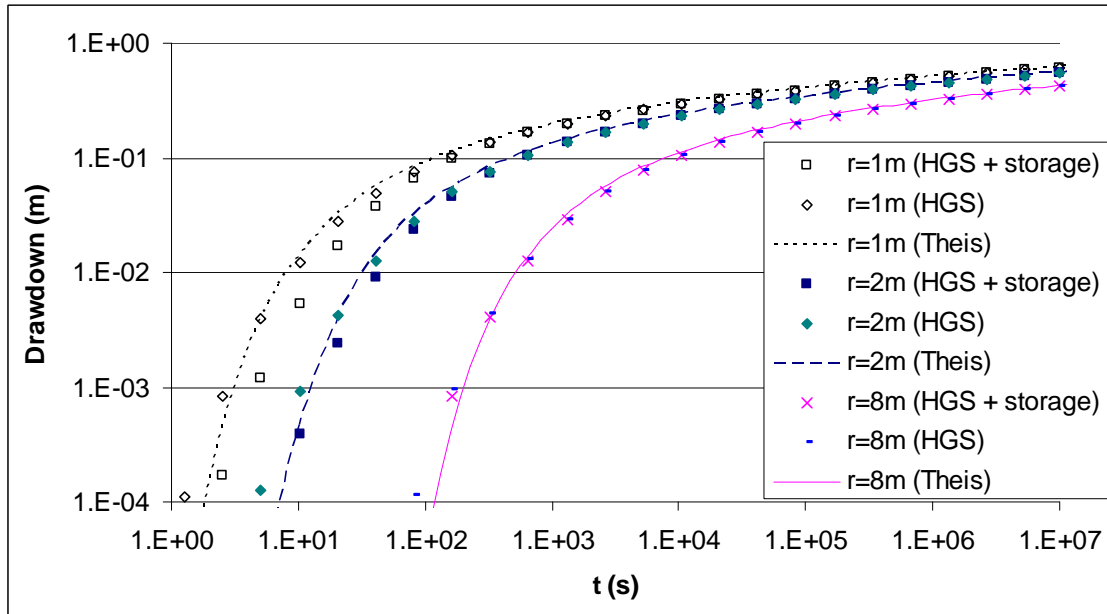


Figure 23 Drawdown at radial distances of 1, 2 and 8 m for pumping in a Theis aquifer, following the code verification example in section 2.3.1. A caisson radius of zero is used in order to remove wellbore storage from the *HGS* calculations. The Theis solution is plotted against *HGS* solutions both with (*HGS + storage*) and without (*HGS*) wellbore storage.